Inactivation of BK Channels by the NH_2 Terminus of the β2 Auxiliary Subunit: An Essential Role of a Terminal Peptide Segment of Three Hydrophobic Residues

Xiao-Ming Xia,[1] J.P. Ding,[1] and Christopher J. Lingle[1,2]

[1]Department of Anesthesiology and [2]Department of Anatomy and Neurobiology, Washington University School of Medicine, St. Louis, MO 63110

ABSTRACT An auxiliary β2 subunit, when coexpressed with *Slo* α subunits, produces inactivation of the resulting large-conductance, Ca^{2+} and voltage-dependent K^+ (BK-type) channels. Inactivation is mediated by the cytosolic NH_2 terminus of the β2 subunit. To understand the structural requirements for inactivation, we have done a mutational analysis of the role of the NH_2 terminus in the inactivation process. The β2 NH_2 terminus contains 46 residues thought to be cytosolic to the first transmembrane segment (TM1). Here, we address two issues. First, we define the key segment of residues that mediates inactivation. Second, we examine the role of the linker between the inactivation segment and TM1. The results show that the critical determinant for inactivation is an initial segment of three amino acids (residues 2–4: FIW) after the initiation methionine. Deletions that scan positions from residue 5 through residue 36 alter inactivation, but do not abolish it. In contrast, deletion of FIW or combinations of point mutations within the FIW triplet abolish inactivation. Mutational analysis of the three initial residues argues that inactivation does not result from a well-defined structure formed by this epitope. Inactivation may be better explained by linear entry of the NH_2-terminal peptide segment into the permeation pathway with residue hydrophobicity and size influencing the onset and recovery from inactivation. Examination of the ability of artificial, polymeric linkers to support inactivation suggests that a variety of amino acid sequences can serve as adequate linkers as long as they contain a minimum of 12 residues between the first transmembrane segment and the FIW triplet. Thus, neither a specific distribution of charge on the linker nor a specific structure in the linker is required to support the inactivation process.

KEY WORDS: inactivation mechanisms • inactivation domains • K^+ channels • BK channels • Ca^{2+}- and voltage-gated K^+ channels

INTRODUCTION

Rapid inactivation of Ca^{2+} and voltage-gated BK-type K^+ channels arises from coexpression of the *slo1* pore–forming α subunits with particular auxiliary β subunits (Wallner et al., 1999; Xia et al., 1999, 2000; Uebele et al., 2000; Lingle et al., 2001). Of the four members of the BK β subunit family, inactivation arises from the short cytosolic NH_2 terminus of either the β2 subunit (Wallner et al., 1999; Xia et al., 1999) or of particular splice variants of the β3 subunit (Uebele et al., 2000; Xia et al., 2000; Lingle et al., 2001). Since *slo1* α and β subunits assemble in a 1:1 stoichiometry (Knaus et al., 1994b; Wang et al., 2002), up to four inactivation-competent NH_2 termini can be present in any inactivating BK channel (Wang et al., 2002). Similar to inactivation of voltage-dependent K^+ (Kv) channels mediated by NH_2-terminal domains of α subunits (MacKinnon et al., 1993; Gomez-Lagunas and Armstrong, 1995), inactivation arises from the independent action of each NH_2 terminus (Xia et al., 1999; Wang et al., 2002). Thus, at least superficially similar elements would appear to contribute both to inactivation of Kv channels and BK channels.

Of the kinetic behaviors exhibited by voltage-gated ion channels, the phenomenon of rapid inactivation of Kv channels has perhaps been most amenable to a correlation of the structural elements of the channel with an actual mechanism of gating. For Kv channels, to produce inactivation, the cytosolic NH_2 terminus, either of the pore-forming α subunits (Hoshi et al., 1990; Ruppersberg et al., 1991) or of cytosolic auxiliary β subunits (Rettig et al., 1994), appears to move into a position that closely abuts the mouth of the ion permeation pathway. The close association of the Kv blocking domain and the ion permeation pathway is supported by the fact that cytosolic channel blockers compete with the blocking domain for occupancy of the channel (Choi et al., 1991; Demo and Yellen, 1991). Furthermore, once the inactivation domain occupies its blocking position, it impedes closure of the channels (Demo and Yellen, 1991; Rup-

Xiao-Ming Xia and J.P. Ding contributed equally to this work.

Address correspondence to C. Lingle, Department of Anesthesiology, Washington University School of Medicine, 600 S. Euclid Ave., Box 8054, St. Louis, MO 63110. Fax: (314) 362-8571; E-mail: clingle@morpheus.wustl.edu

J. Gen. Physiol. © The Rockefeller University Press • 0022-1295/2003/02/125/24 $8.00
Volume 121 February 2003 125–148
http://www.jgp.org/cgi/doi/10.1085/jgp.20028667

persberg et al., 1991). Yet, until recently the nature of the interaction between any inactivation domain and its target site has remained elusive. Now, an important advance has been the demonstration that the initial first four residues of the NH_2 terminus of an inactivating Kvβ auxiliary subunit interact with specific residues in the pore-forming S6 segment of the Kv 1.4 α subunit (Zhou et al., 2001). Thus, the initial residues of an inactivating NH_2 terminus appear to snake their way into the permeation pathway to occlude ion flux.

To what extent this molecular picture of Kv inactivation may apply to BK channels remains unclear. Several functional properties of BK inactivation clearly differ from Kv inactivation. For example, BK channel inactivation is not slowed by cytosolic blockers that bind to the mouth of the BK channel pore (Lingle et al., 1996; Solaro et al., 1997; Xia et al., 1999). Furthermore, unlike Kv inactivation (Demo and Yellen, 1991; Ruppersberg et al., 1991), BK channels do not reopen during recovery from inactivation, suggesting that when the inactivation domain resides in its blocking position, BK channels are not prevented from undergoing a normal open to closed conformational change (Solaro et al., 1997). These properties of BK channel inactivation seem more reminiscent of Na^+ channel inactivation, in which occupancy by blockers of sites within the pore do not interfere with the inactivation mechanism (O'Leary and Horn, 1994; Kuo and Liao, 2000). However, BK channel inactivation shares with both *Shaker*B K^+ channels (Gomez-Lagunas and Armstrong, 1994) and voltage-dependent Na^+ channels (Kuo and Liao, 2000) a dependency on the concentration of extracellular permeant ions (Solaro et al., 1997). Thus, both similarities and differences exist between the rapid inactivation properties of BK channels and Kv channels and the extent to which the underlying molecular mechanism is similar is yet unresolved.

An additional challenge to our current understanding of rapid inactivation, both for Kv channels and BK channels, is that inactivation may involve kinetic complexity not previously accounted for by the simple, one-step open channel block model generally used to describe inactivation. Specifically, inactivation of BK channels mediated by the β3b subunit involves two kinetic steps (Lingle et al., 2001) and a similar model has also been proposed for inactivation of Kv channels by NH_2-terminal inactivation domains (Zhou et al., 2001). For Kv channels, it was proposed that perhaps an initial movement of the inactivation structure (first step) then permits the hydrophobic blocking domain to enter the channel (second step) (Zhou et al., 2001). As part of this conceptualization, the first kinetic step was proposed to depend on the interaction of charged NH_2-terminal residues with charged residues lining the entryway to the channel, thereby appropriately positioning the hydrophobic segment for blockade. However, as yet there are no specific experimental results that support the idea that inactivation of Kv channels occurs with two distinct kinetic steps or to associate charge on the NH_2 terminus with a particular kinetic step. Similarly, the physical basis of each of the two kinetic steps involved in BK channel inactivation remains unknown (Lingle et al., 2001).

As part of our efforts to understand BK channel inactivation and to resolve the functional and structural differences between inactivation of Kv channels and BK channels, here we have undertaken a mutational analysis of inactivation of BK channels mediated by the β2 auxiliary subunit. The NH_2 terminus of the β2 subunit of the BK channel family contains 46 amino acids that are considered to be cytosolic to the first transmembrane (TM)* segment (Wallner et al., 1999; Xia et al., 1999). For comparison, the noninactivating β1 subunit (Knaus et al., 1994a) contains 15 cytosolic residues many of which are homologous to their counterparts (residues 31–45) in the β2 subunit.

We address two different aspects of the role of the β2 NH_2 terminus. First, we define the key segment of residues involved in producing inactivation. Second, we address the role of the linker between the key inactivation epitope and the first transmembrane segment (TM1) of the β2 subunit. Our results clearly establish that residues 2–4 (FIW) of the NH_2 terminus are the critical inactivation epitope in the β2 subunit. This critical inactivation segment appears to be both necessary and sufficient to produce inactivation. Our results also show that deletions involving residues from positions 4 through 36 are of minimal impact on the ability of the β2 subunit to inactivate. Additional examination of the properties of the linker between the FIW epitope and TM1 shows that neither charge nor maintenance of any particular structural integrity conferred by residues from positions 5 through 41 is required to permit inactivation to occur. Thus, inactivation mediated by the β2 subunit simply requires a set of three hydrophobic residues linked to TM1 by a spacer of rather nonspecific requirements.

MATERIALS AND METHODS

Site-directed Mutagenesis

The pfu DNA polymerase was used in all PCRs to generate hβ2 mutations and all constructs were verified by sequencing (Stratagene). In general, strategies followed standard procedures in use in this laboratory (Xia et al., 1998b, 1999). Here we explicitly describe procedures for generation of five categories of mutation employed in this paper: first, constructs with deletions in the NH_2 terminus; second, constructs with mutations of residues within or near the initial four residues of the NH_2 terminus; third, constructs with glutamine insertions; fourth, point mutations of charged residues; and fifth, constructs with artificial NH_2 termini.

Abbreviation used in this paper: TM, transmembrane.

Deletion Constructs

β2 NH_2-terminal deletion constructs were generated by pfu PCR with two specific β2 primers. For example, to generate Δ2–4 (ΔFIW), a PCR was performed with pfu polymerase (primers 5′-ATCAGAATTCTCTAAGATGAGTGGCCGGACCTCTTCATC-3′ and 5′-TACTAGTCGACAAAAATTATTTTATCCATTTTTG-3′). The product was then digested with EcoRI and SalI, and then ligated into EcoRI-SalI vector pBF. The deletion was verified by sequencing. Other deletions were obtained in a similar fashion.

Mutations of Residues within the Initial Four Residues

For mutations within the initial FIW region, a pair of complementary primers was used to generate each mutation. The primers contained the designated changes of codons (e.g., F to G, I to G, W to G). The PCR was performed on wild-type hβ2 template (96°C for 2 min; 17–20 cycles of 96°C for 30 s, 50°C for 45 s, 68°C for 10 min; 96°C for 2 min). The reaction product was digested with DpnI for 2–3 h at 37°C, and then transformed to *E. coli* strain DH5α (Xia et al., 1998a). Mutants were identified by DNA miniprep and subsequently sequenced.

Insertion of a Glutamine Chain

Insertion of a chain of glutamine residues (poly-Q) was generated by linking two PCR fragments and subcloning into the oocyte expression vector pBF (Xia et al., 1998a). As an example, to generate the insertion of a 14 amino acid insert at position 46 (INS@46), two PCRs, A and B, were performed each with specific primers (A, 5′-ATCAGAATTCAGACCCTGGACCAACATTCTCTAAG-3′ + 5′-CGGGATCCCTGCTGCTGCTGCTGCTGTCGGTCCTCTCCTGC-CTTCAG-3′; B, 5′-GAAGATCTCAACAACAACAACAACAACGAGC-TATTCTCCTGGGACTG-3′ + 5′-TACTAGTCGACAAAAATTATTT-TATCCATTTTTG-3′). The products were then purified with QIAGEN column, digested with EcoRI + BamHI (reaction A), and BglII + SalI (reaction B) overnight. After gel purification, three fragments, A + B + EcoRI-SalI vector pBF, were incubated for overnight ligation at 16°C, and then the ligation reaction was transformed to *E. coli* strain DH5α. Clones with the correct insert size were identified by EcoRI + SalI digestion and then sequenced for verification. This generates the 14 amino acid insertion of QQQQQQGSQQQQQQ after the amino acid at position 45. Similar insertions were made following residues 8, 15, 27, and 35.

Point Mutations of Charged Residues

As an example of how point mutations of charged residues were generated, here generation of K33Q is described. Two complementary primers were synthesized (5′-CATGACCTCCTGGAC-**CAA**AGGAAAACAGTCACA-3′ and 5′-TGTGACTGTTTTCCT**T-TG**GTCCAGGAGGTCATG-3′), in which nucleotides at the site of the targeted codon were changed to nucleotides encoding the designated amino acid codon (AAA to CAA). The PCR was performed on pBF-hβ2 template (96°C 2 min; 17–20 cycles of 96°C for 30 s, 50°C for 45 s, 68°C for 10 min; 96°C for 2 min), and the product was digested with DpnI for 2–3 h at 37°C, and then transformed to *E. coli* strain DH5α (Xia et al., 1998a). Single colonies were picked up for a subsequent DNA miniprep and sequencing was applied for mutant identification. Multiple point mutations could be obtained by repeating several rounds of the above.

Generation of Artificial NH_2 Termini

The artificial NH_2 termini, such as FIW-8Q, were generated by pfu PCR with a set of primers. The NH_2-terminal primer contained nucleotides encoding FIW-8Q after an initial ATG and then β2 sequence from TM1 with a EcoRI site at 5′ (5′-ATGAATTCTCTAAGATGCAGCAACAACAACAACAACAACGA-GCTATTCTCCTGGGAC-3′); the COOH-terminal primer matched antisense sequence around the β2 stop codon with a 5′ SalI site (5′-ATCGTCGACAAAAATTATTTTATCCATTTTTGCAT-3′). The 634bp PCR fragment was purified, digested with EcoRI and SalI, cloned into pBF, and then verified by sequencing. The longer poly-Q chain constructs were generated by similar methods, although the shorter poly-Q chain constructs were used as the PCR template.

Expression in Xenopus Oocytes

SP6 RNA polymerase was used to synthesize cRNA for oocyte injection after DNA was linearized with MluI (Xia et al., 1999). 50 nl of cRNA (10–20 ng/μl) was injected into stage IV *Xenopus* oocytes harvested 1 d before. To ensure saturation of each BK channel with β subunits, we injected α and β subunits at ratios of at least 1:2 by weight.

Electrophysiological Recording

Recordings from inside-out patches (Hamill et al., 1981) followed standard procedures in use in this laboratory (Xia et al., 1999; Lingle et al., 2001; Zhang et al., 2001). Currents were typically digitized at 10–20 kHz (Bessel low-pass filter; −3 dB). The pipette extracellular solution was (in mM) 140 potassium methanesulfonate, 20 KOH, 10 HEPES, and 2 $MgCl_2$, pH7.2. The usual test solution bathing the cytoplasmic face of the patch membrane contained (in mM) 140 potassium methanesulfonate, 20 KOH, 10 HEPES, pH 7.0, and 5 mM HEDTA with Ca^{2+} -methanesulfonate added to make 10 μM free Ca^{2+}. Procedures for preparation of solutions with defined [Ca^{2+}] have been described (Zeng et al., 2001; Zhang et al., 2001) and the solution applied over the cytosolic face of excised patches was controlled by a local perfusion system (Solaro et al., 1995, 1997). Voltage commands and the acquisition of currents were accomplished with pClamp 7.0 for Windows (Axon Instruments, Inc.).

The Evaluation of Inactivation Behavior of Different Mutant Constructs

For all constructs, the following functional characteristics were determined: (a) the G-V curve at 10 μM Ca^{2+} measured from peak current and also, for noninactivating variants, from tail current; (b) the time constant of inactivation (τ_{on}) at potentials from 40 through 160 mV at 10 μM Ca^{2+}; and (c) the time constant of recovery (τ_{off}) from inactivation at −140 mV with 10 μM Ca^{2+}. In addition, for some constructs, there was appreciable steady-state current at potentials where inactivation mediated by the β2 subunit is essentially complete. In such cases, f_{ss}, the fractional amplitude of steady-state current relative to maximal activatable current (I_{max}), was determined. f_{ss} is potentially indicative of the equilibrium between blocking and unblocking transitions. I_{max} was determined in two ways: first, from fitting the current time course to a function including terms for both activation and inactivation and, second, from application of trypsin to directly define I_{max}. In cases where each method could be applied to the same constructs, both estimates of I_{max} were within 10%.

$$O \underset{k_{-1}}{\overset{k_1}{\rightleftharpoons}} I$$

SCHEME I

$$O \underset{k_{-1}}{\overset{k_1}{\rightleftharpoons}} O^* \underset{k_{-2}}{\overset{k_2}{\rightleftharpoons}} I$$

SCHEME II

The empirical measures of channel inactivation behavior, τ_{on}, τ_{off}, and f_{ss} are most useful if they can be related to specific molecular transitions in a blocking scheme.

The standard scheme used to characterize either inactivation or blockade by NH_2-terminal inactivation peptides is given in Scheme I. However, more recently it has been shown that inactivation mediated by the β3b subunit involves two distinct kinetic steps (Lingle et al., 2001) and other work now shows that a similar model is also necessary to account for β2 subunit–mediated inactivation (unpublished data). This model, given in Scheme II, involves formation of a preinactivated open state (O*) that precedes entry into inactivated states. A similar kinetic mechanism has been proposed to explain inactivation of Kv channels (Zhou et al., 2001), although direct evidence demonstrating the existence of two kinetic steps for Kv channels is still lacking. Because of the fact that Scheme II almost certainly applies to the mechanism of inactivation studied here (and perhaps to that of Kv channels; Zhou et al., 2001), there is simply no explicit way with the parameters we can measure to make definitive estimates of the underlying molecular transitions and the energetic changes caused by any given mutation. However, in lieu of such specific mechanistic information, here we employ three different empirical measures of the inactivation behavior that are of use in comparing the consequences of mutations.

First, for each construct we define $\ln[\tau_{on(mut)}/\tau_{on(\beta2)}]$ and $\ln[\tau_{off(mut)}/\tau_{off(\beta2)}]$, which allow comparison of the consequences of each mutation relative to the wild-type β2 subunit in terms of units of kT. Irrespective of the molecular steps in the inactivation process, it is likely that τ_{on} at least qualitatively reflects primarily the factors that influence association of any inactivation domain with its blocking site while τ_{off} measured at −140 mV reflects, at least in part, dissociation of the inactivation domain. This approach has been also been used to evaluate the interaction of a Kv inactivation domain with the Kv1.4 α subunit, in which it has also been proposed that a two-step mechanism of inactivation applies (Zhou et al., 2001). Irrespective of the mechanism of inactivation, $\ln[\tau_{on}/\tau_{on(\beta2)}]$ and $\ln[\tau_{off}/\tau_{off(\beta2)}]$ provide model-independent indicators of changes in the inactivation process that allows comparison among constructs.

Second, to allow comparison between constructs in which both τ_{on} and τ_{off} may change, we also determine $\ln[(\tau_{on(mut)}/\tau_{off(mut)})/(\tau_{on(\beta2)}/\tau_{off(\beta2)})]$, which yields a measure in units of kT of the amount of change in the stability of the inactivated state relative to the wild-type β2 subunit. For inactivation of Kv1.4 by various mutations of the Kvβ2 NH_2 terminus, which is also proposed to involve a similar two-step inactivation mechanism, $\ln[(\tau_{on(mut)}/\tau_{off(mut)})/(\tau_{on(\beta2)}/\tau_{off(\beta2)})]$ has been equated to $\ln[K_{d(mut)}/K_{d(wt)}]$ (Zhou et al., 2001). Although it is likely that the relative changes in this estimate of $\ln[K_{d(mut)}/K_{d(wt)}]$ caused by any mutation do reflect something about the true equilibrium constants of the inactivation process, they are clearly not true equilibrium constants, both because inactivation probably involves two steps and because inactivation onset and recovery are measured at different voltages. Yet, as one tool for comparing the consequences of any given mutation, this formulation is still useful. Here we use the term "inactivation stability" defined as $K^* = \tau_{on}/\tau_{off}$ for any given construct, such that $\ln[K^*_{mut}/K^*_{\beta2}] = \ln[(\tau_{on(mut)}/\tau_{off(mut)})/(\tau_{on(\beta2)}/\tau_{off(\beta2)})]$. The parameter, $\ln[K^*_{mut}/K^*_{\beta2}]$, which is in kT units, provides a sense of the magnitude of the overall energetic changes that arise from any given mutation, although it should not be taken as a true equilibrium constant. $\ln[K^*_{mut}/K^*_{\beta2}]$ should probably be considered less useful when a construct exhibits appreciable steady-state currents (larger f_{ss}) at 100 mV.

Finally, as an additional tool for assessing inactivation stability among various constructs, we take advantage of both τ_{on} and f_{ss}. Scheme I allows explicit characterization of the underlying rates k_1 and k_{-1}, as given in the following pair of equations (Murrell-Lagnado and Aldrich, 1993b):

$$\tau_{on} = 1000/(k_1 + k_{-1}).$$

$$f_{ss} = k_{-1}/(k_1 + k_{-1}).$$

Thus, from Scheme I, the above equations provide a means of evaluating the effects of particular mutations directly on both the molecular association rate and the dissociation rate (Murrell-Lagnado and Aldrich, 1993b), where $k_1 = 1{,}000/\tau_{on} - k_{-1}$ and $k_{-1} = f_{ss}*1000/\tau_{on}$. From this, we define an inactivation equilibrium constant, $K = k_{-1}/k_1$. Relative to wild-type β2 behavior, this yields $\ln[K_{mt}/K_{\beta2}]$. Although f_{ss} is poorly defined for wild-type α + β2 currents, since the same value of $K_{\beta2}$ is used for calculation of all estimates of $\ln[K_{mt}/K_{\beta2}]$, it remains a useful tool for comparison among constructs. If a construct behaves in accordance with Scheme I, in which K defines a true binding affinity, $\ln[K_{mt}/K_{\beta2}]$ defines the change in free energy of binding ($\Delta\Delta G_{mt-\beta2}$) resulting from the mutation. For Scheme II, although K is not a true equilibrium constant, $\ln[K_{mt}/K_{\beta2}]$ provides a simple qualitative estimate of the change in apparent efficacy of the inactivation process which is useful for comparison of different constructs, particularly when steady-state currents are appreciable.

It should be noted that $\ln[K^*_{mt}/K^*_{\beta2}]$ and $\ln[K_{mt}/K_{\beta2}]$, although both reflect something about the stability of the inactivation mechanism, are calculated from different conditions and, although relative changes between constructs would be expected to be similar, exact values are expected to differ.

FIGURE 1. Sequence of NH_2 termini of the BK auxiliary β subunit family. (A) NH_2 termini of the four known auxiliary β subunits are shown. For the β3 subunit for which four alternatively spliced NH_2 termini have been identified (Uebele et al., 2000), the rapidly inactivating β3b variant is shown. TM1 designates the proposed beginning of the first TM segment. Positive and negative residues in the β2 subunit are in blue and red, respectively. Boxed sets of β2 residues (11–17 and 20–30) are thought to adopt relatively helical structures in an isolated peptide, while other portions of the NH_2 terminus are relatively disordered (Bentrop et al., 2001). (B) The initial 20 residues of several inactivating NH_2 termini are compared, showing the common theme of a hydrophobic segment at the NH_2 terminus and the downstream hydrophilic region.

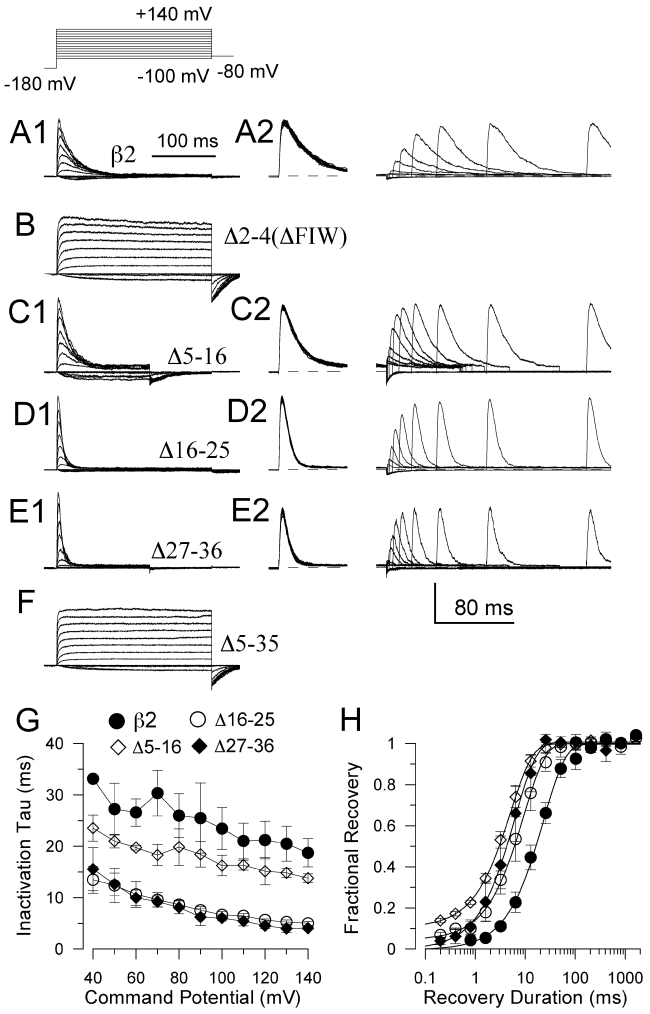

FIGURE 2. Deletions spanning positions 5–36 do not abolish inactivation. In A1, currents resulting from α subunits coexpressed with wild-type β2 subunits were activated by the indicated voltage protocol. In A2, currents were activated by a paired pulse protocol (activation steps to 100 mV) separated by steps of different duration to −140 mV. Currents during the initial activation step were truncated to allow better visualization of the recovery time course. In B, removal of Phe, Ile, and Trp in positions 2–4 (ΔFIW) results in removal of inactivation. In C1 and C2, currents arising from a β2 subunit with amino acids in positions 5–16 deleted (Δ5–16) are shown. The first 10 amino acids in this construct are MFIWEKRNIY. Note the steady-state current in this construct that may arise from the influence of charged residues in positions 5–7. In D1 and D2, currents arising from a construct with residues 16–25 deleted (Δ16–25) are shown. In E1 and E2, currents are shown for a construct with residues 27–36 deleted (Δ27–36). In F, the currents show that deletion of residues 5 through 35 (Δ5–35) results in removal of inactivation. In Δ5–35, the total length of the cytosolic portion of the NH_2 terminus is 14. In G, inactivation time constants (τ_{on}) for β2 (●, 4 patches), Δ5–16 (◇, 3 patches), Δ16–25 (○, 4 patches), and Δ27–36 (◆, 4 patches) are plotted as a function of activation potential showing a similar weak voltage-dependence of τ_{on} for each construct. Each point is the mean and SD of 4–7 patches. In H, the recovery time course at −140 mV defined from the paired pulse protocol is shown for a set of patches for each construct. For β2 (●, 4 patches), the fitted τ_{off} is 23.4 ± 2.3 ms; for Δ5–16 (◇, 3 patches), τ_{off} is 5.13 ± 0.19 ms; for Δ16–25 (○, 4 patches), τ_{off} is 9.30 ± 0.55 ms; for Δ27–36 (◆, 3 patches), τ_{off} is 6.19 ± 0.33 ms. Vertical calibration bar corresponds to: A1, 3 nA; A2, 2 nA; B, 6 nA; C1, 4 nA; C2, 3 nA; D1, 6 nA; D2, 4 nA; E1, 1.5 nA; E2, 1.2 nA; F, 8 nA.

RESULTS

Properties of the β2 NH_2 Terminus

The sequence of the β2 NH_2-terminal residues that precedes the predicted first TM1 is given in Fig. 1 along with the NH_2-terminal residues for other BK β subunits. The β2 NH_2 terminus consists of a total of 46 residues, including the initiation methionine that extend cytosolically from the beginning of the postulated TM1 sequence. The NH_2 terminus contains six positive and four negative amino acids in the first thirty amino acids, resulting in a net charge on the initial 31 amino acids of +2, ignoring the terminal methionine. β2 sequence following the initial 31 residues shares similarity with the β1 NH_2 terminus, which does not exhibit inactivation. Thus, residues in positions 31–46 of the β2 subunit are unlikely to participate directly in inactivation.

An NMR structure of an isolated β2 NH_2-terminal peptide has been determined (Bentrop et al., 2001). Two segments of the NH_2 terminus exhibited a reasonably stable structure in solution, indicated by the boxed residues in Fig. 1 A. The first 10 relatively hydrophobic residues exhibit large flexibility, as do residues downstream of position 31.

The β2 subunit shares some common features with many other NH_2-terminal inactivation domains of both α and β subunit of Kv channels. In general, a segment of largely hydrophobic residues (Fig. 1 B) is followed by a more hydrophilic segment often containing both positive and negative charges. Among different NH_2 termini, there is no clear pattern of charge, although most inactivating NH_2 termini contain net positive charge.

Deletion of Amino Acids in Positions 2–4, but not in Positions 5–31, Abolish Inactivation

Our first goal was to define residues or regions of the NH_2 terminus of the β2 subunit that might be critical to the inactivation process. Therefore, a series of constructs was generated in which residues were deleted from various positions in the NH_2 terminus. Two protocols were used to characterize each construct: first, an activation protocol involving a depolarizing command step to various potentials from −100 through 180 mV and, second, a paired pulse recovery protocol in which two depolarizing voltage steps to 100 mV were separated by a variable recovery interval at −140 mV. As shown in Fig. 2 A1 for wild-type β2 currents, the activation proto-

TABLE I

Effects of NH_2-terminal Deletions Over Positions 5–36

Construct	τ_{on}	$\ln(\tau_{on(mt)}/\tau_{on(\beta2)})$	τ_{off}	$\ln(\tau_{off(mt)}/\tau_{off(\beta2)})$	$\ln[K^*_{mut}/K^*_{\beta2}]$	f_{ss}	$\ln[K_{mt}/K_{\beta2}]$	*n*
	ms	*[kT]*	*ms*	*[kT]*	*[kT]*		*[kT]*	
β2 (1:1)	23.7 ± 2.9	—	21.9 ± 4.8	—		0.005	—	10
ΔF	13.3 ± 0.6	−0.578	4.3 ± 0.6	−1.628	1.05	0.018	1.29	6
ΔFI	9.8 ± 1.2	−0.883	2.3 ± 0.3	−2.254	1.37	0.204	3.93	8
ΔFIW[1]	none	—	none	—	—	—	—	8
ΔFIWT	none	—	none	—	—	—		10
Δ5–6	27.6 ± 2.2	0.152	28.7 ± 4.0	0.270	−0.12	0.007	0.34	4
Δ5–8	25.8 ± 4.3	0.0849	26.2 ± 6.1	0.179	−0.094	0.007	0.34	7
Δ5–12	46.7 ± 4.5	0.678	63.6 ± 3.7	1.066	−0.39	0.024	1.59	6
Δ5–16	15.6 ± 1.1	−0.418	4.7 ± 0.8	−1.539	1.13	0.05	2.34	7
Δ5–20	101 ± 7	1.334	33.4 ± 4.3	0.865	0.47	0.11	3.20	4
Δ5–24	35.5 ± 3.8	0.404	31 ± 0.6	0.348	0.057	0.59	5.66	5
Δ5–35	none	—	none	—	—	—	—	7
Δ27–36	5.4 ± 0.6	−1.479	6.3 ± 1.7	−1.246	−0.23	0.004	0.22	4
Δ16–20	34.5 ± 5.1	0.375	37.8 ± 4.3	0.546	−0.17	0.014	1.04	4
Δ16–25	7.9 ± 0.9	−1.099	10.0 ± 3.0	−0.784	−0.32	0.008	0.47	4

[1]Trypsin did not increase current at 140 mV.

col allows measurement of a time constant of inactivation (τ_{on}) at different potentials and also the fraction of noninactivating current at steady-state (f_{ss}) at a given potential. The paired pulse protocol (Fig. 2 A2) yields a time constant of recovery from inactivation (τ_{off}).

The main observation from the deletion constructs was that deletion of amino acids in positions 2–4 (Δ2–4; ΔFIW) removes inactivation (Fig. 2 B). Inactivation was also completely abolished in two other constructs in which residues 2–4 were removed: constructs Δ2–5 and Δ2–10. In contrast, deletions of various segments spanning amino acid positions 5 through 36 all permit relatively complete inactivation to occur (Fig. 2, C–E), although changes in both τ_{on} (Fig. 2 G) and τ_{off} (Fig. 2 H) are observed. For example, deletion of residues 16–25 (Δ16–25) results in both a faster τ_{on} (at 100 mV) and a faster τ_{off} (at −140 mV) compared with inactivation mediated by the wild-type β2 NH_2 terminus. With the deletion of 31 residues (Δ5–35), inactivation disappeared (Fig. 2 F). The similarity of the $V_{0.5}$ for activation for β2 wild-type and the Δ5–35 construct indicates that the construct was expressed. Since other deletion mutations that span the range of residues 5–35 do permit inactivation, the failure of Δ5–35 to inactivate probably reflects the length of the NH_2 terminus, as shown below. Table I summarizes the effects of various deletions on τ_{on} and τ_{off}, and expresses those values relative to the wild-type β2 subunit (see MATERIALS AND METHODS). Of the deletions other than Δ2–4 and Δ5–35, it should be noted that deletions Δ5–20 and Δ5–24 were the most effective in altering the inactivation process, although in both cases inactivation can still occur.

We next examined more closely the consequences of deletion of residues in the FIW segment. The effects of deleting one (ΔF) and two (ΔFI) residues after the initiation methionine are shown in Fig. 3, B and C. Removal of each amino acid progressively reduced the apparent stability of the inactivation process. In ΔF and ΔFI, both τ_{on} and τ_{off} were faster than for wild-type α + β2 currents (Fig. 3, D and E). It should be noted that recovery from inactivation of both of these constructs shows evidence of time-dependent changes in the instantaneous current-voltage curve, consistent with previous work on α + β3b currents (Lingle et al., 2001), supporting the two-step model of inactivation (see MATERIALS AND METHODS, Scheme II). Thus, although dissociation of the NH_2 terminus from a binding site certainly contributes to the recovery time course, dissociation is probably not the sole determinant of the observed recovery time course.

To verify that the loss of inactivation reflected some specific properties of the FIW residues rather than a simple shortening of the NH_2 terminus, several alternative constructs were examined. When FIW was replaced with GGG, inactivation was also abolished (Fig. 4 A). Similarly, replacement of FIWTS with GGGGG also abolished inactivation. We also introduced GGG both before (GGGFIW; Fig. 4 B) and after (FIWGGG; Fig. 4 C) FIW. In both cases, the NH_2 terminus remained inactivation competent, although the apparent affinity of the inactivation process was reduced. Thus, the loss of inactivation when FIW was replaced by GGG is not simply an inhibitory effect of GGG, but reflects a specific role of the FIW residues in inactivation (summarized in Table II). On balance, whether judged by removal of

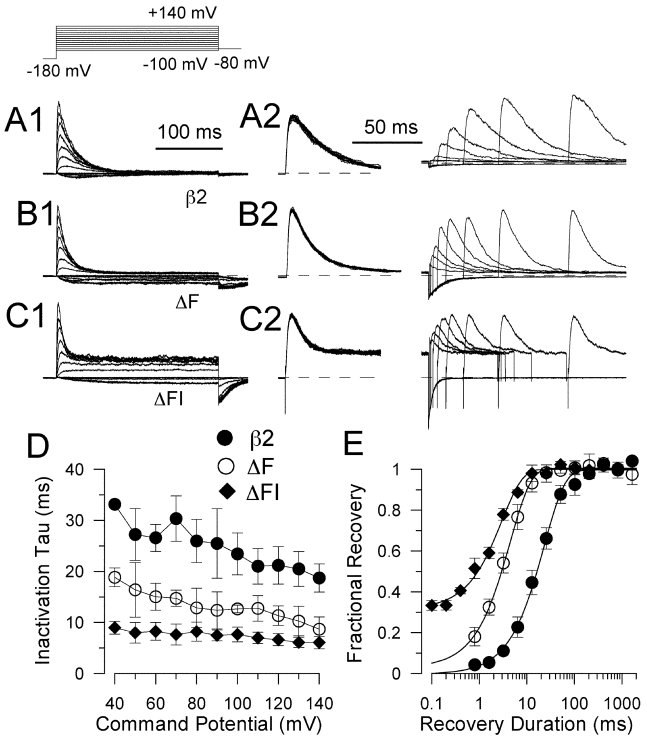

FIGURE 3. Deletions within positions 2–4 of the NH_2 terminus reduce and abolish inactivation. In A1, activation of wild-type α + β2 currents are illustrated while, in A2, the time course of recovery from inactivation at −140 mV is shown. In B1 and B2, currents resulting from a construct with deletion of Phe in position 2 (ΔF) are shown, along with the time course of recovery from inactivation for that construct. Note the appearance of some steady-state current at all activation potentials. In C1 and C2, currents resulting from a construct with deletion of Phe and Ile in positions 2 and 3 (ΔFI) are shown. More substantial steady-state current is observed along with more rapid recovery from inactivation. In D, τ_{on} is plotted as a function of activation potential for each of the three inactivating constructs (β2: ●, 4 patches; ΔF: ○, 4 patches; ΔFI, ◆, 8 patches). In E, the time course of recovery from inactivation determined at −140 mV is illustrated for the three constructs. For β2, τ_{off} is given in Fig. 2; for ΔF (3 patches), τ_{off} is 4.5 ± 0.3 ms; for ΔFI (4 patches), τ_{off} is 2.99 ± 0.33 ms.

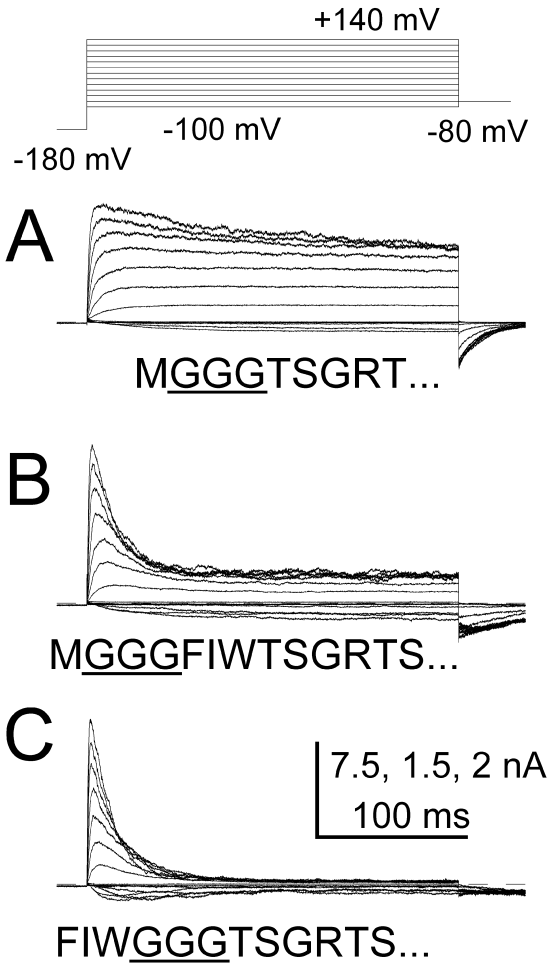

FIGURE 4. Consequences of replacement or displacement of FIW residues with GGG. In A, currents arising from a construct in which residues FIW were replaced with GGG are shown. No inactivation is observed, and trypsin application resulted in no increase in outward current. In B, currents are shown for a construct in which GGG was appended to the initial FIW sequence. The apparent stability of inactivation is reduced, but inactivation still occurs. In C, currents are shown for a construct in which GGG was inserted between FIW and the remainder of the NH_2 terminus. In this case, steady-state inactivation is than for wild-type, but still substantial.

visible inactivation, by a larger steady-state current (f_{ss}), or by faster τ_{off}, mutations in this region generally cause more severe alterations in inactivation than the much more sizable deletions from position 5 through 36 summarized in Table I. Thus, the FIW segment appears to be the critical element required to maintain relatively normal inactivation.

Inactivation Efficacy Correlates with Bulk Hydrophobicity in the Inactivation Triplet

We next examined the role of the amino acids in the FIW triplet. First, having shown that replacement of FIW with GGG fails to inactivate, we mutated each residue to G either singly or in pairs. Second, the consequences of changing the distance between F and W were examined with the introduction of either G or negative charges as spacers. Third, each residue was mutated either to E or R to examine the role of introduction of charge in this region. Fourth, we examined the consequences of making all residues identical, as in III, FFF, or WWW. Fifth, we altered the order of FIW within the triplet. Results from these constructs are summarized in Table II.

Currents from constructs in which each of the three NH_2-terminal residues were substituted with glycine are shown in Fig. 5, B–D. In each case, introduction of a single glycine, although weakening the apparent affinity of the inactivation process, did not abolish the inac-

TABLE II

Consequences of Various Mutations Affecting the FIW Triplet

Construct	τ_{on} + 100 mV	$\ln(\tau_{on(mt)}/\tau_{on(\beta2)})$	τ_{off} − 140 mV	$\ln(\tau_{off(mt)}/\tau_{off(\beta2)})$	$\ln[K^*_{mut}/K^*_{\beta2}]$	f_{ss}	$\ln[K_{mt}/K_{\beta2}]$	*n*
	ms	*[kT]*	*ms*	*[kT]*	*[kT]*		*[kT]*	
β2	23.7 ± 2.9		21.9 ± 4.8			0.005		10
GGGFIWTS...	22.3 ± 5.3	−0.061	5.5 ± 1.4	−1.38	1.32	0.26	4.24	4
FIWGGGTS...	23.2 ± 2.6	−0.021	14.3 ± 1.5	−0.43	0.40	0.015	1.11	4
GGGTS...	none	—	none	—	—	—		5
GGGGGTS...	none	—	none	—	—	—		5
FGGW	24.0 ± 4.6	0.013	4.7 ± 0.6	−1.54	1.55	0.064	2.61	3
FGGGW	17.7 ± 1.2	−0.292	4.6 ± 0.8	−1.560	1.27	0.06	2.54	6
FGGGGW	16.4 ± 0.5	−0.368	3.9 ± 0.7	−1.726	1.36	0.26	4.24	4
LIW	20.9 ± 1.7	−0.126	11.4 ± 1.1	−0.65	0.53	0.02	1.40	7
−IW	13.3 ± 0.6	−0.578	4.3 ± 0.6	−1.63	1.05	0.022	4.14	4
RIW	15.0 ± 2.7	−0.457	2.9 ± 0.6	−2.02	1.56	0.14	3.48	4
AIW	14.2 ± 0.8	−0.512	2.6 ± 0.3	−2.13	1.62	0.04	2.12	4
GIW	17.1 ± 3.8	−0.548	2.1 ± 0.4	−2.50	1.95	0.15	3.56	6
EIW	9.3 ± 0.7	−0.935	1.3 ± 0.1	−2.82	1.89	0.35	6.05	4
FTW	16.7 ± 1.6	−0.350	13.1 ± 2.3	−0.51	0.16	0.21	1.45	4
FAW	23.0 ± 2.5	−0.030	8.0 ± 0.8	−1.01	0.98	0.01	0.70	4
FRW	26.2 ± 2.3	0.100	7.3 ± 0.3	−1.10	1.20	0.02	1.40	3
FGW	13.8 ± 0.8	−0.541	8.8 ± 1.6	−0.91	0.37	0.039	2.09	4
FEW	11.0 ± 0.8	−0.768	3.9 ± 0.5	−1.73	0.96	0.273	4.31	4
- - W	9.8 ± 1.2	−0.883	2.3 ± 0.2	−2.25	1.37	0.024	1.29	8
FIL	13.8 ± 2.1	−0.541	21.7 ± 4.7	−0.01	−0.53	0.11	3.20	4
FIA	8.8 ± 0.6	−0.991	4.2 ± 0.6	−1.65	0.66	0.09	2.98	5
FIR	10.7 ± 1.5	−0.795	3.3 ± 0.8	−1.89	1.10	0.049	2.12	4
FIG	9.8 ± 1.2	−0.883	4.9 ± 0.5	−1.50	0.61	0.09	2.98	5
FIE	6.5 ± 0.9	−1.294	1.3 ± 0.2	−2.82	1.53	0.32	4.40	5
WIF	39.3 ± 3.5	0.506	20.0 ± 3.3	−0.10	0.60	0.023	1.54	5
FWI	29.9 ± 2.7	0.232	τ_f: 6.5 ± 0.6 τ_s: 323 ± 46	−1.21	1.45	0.013	0.96	5
IWF	37.2 ± 3.9	0.451	13.5 ± 2.2	−0.48	0.93	0.025	1.63	5
GGW	6.0 ± 0.7	−1.374	0.49 ± 0.08	−3.80	2.43	0.656	5.94	6
FGG	9.8 ± 1.9	−0.883	1.4 ± 0.3	−2.75	1.87	0.39	5.29	4
GIG	none		none					5
III	12.9 ± 2.2	−0.608	3.6 ± 0.4	−1.81	1.20	0.12	3.30	4
FFF	33 ± 1	0.331	16.7 ± 3.1	−0.27	0.60	0.018	1.29	5
WWW	132 ± 17	1.717	43 ± 11	0.68	1.04	0.025	1.63	5
FDEW	none		none					3
FDDEW	none		none					4
FDDDEW	none		none					3

tivation process. With two glycines (Fig. 5, E–G), the efficacy of the inactivation process was further reduced. However, either a single F or single W were sufficient to maintain some inactivation, while construct GIG did not exhibit inactivation. This suggests that residues F and W and/or positions 2 and 4 are more critical to the stability of the inactivated state than residue I in position 3.

The effects of varying the distance between F and W either with G or with negatively charged residues are shown in Fig. 5, H–K. Even with up to four Gs inserted between F and W, inactivation is maintained. With FGGWTS, the fraction of steady-state noninactivating current (f_{ss}) at 100 mV is less than in FGGTS, suggesting that W may contribute to the apparent affinity of the inactivation process. When two or three glycines are inserted between F and W (FGGWTS and FGGGWTS), the extent of inactivation is more comparable to FGGTS, although the presence of W still appears to influence inactivation stability to some extent. In contrast to the results with insertion of glycine residues, when two or more negatively charged residues are used as

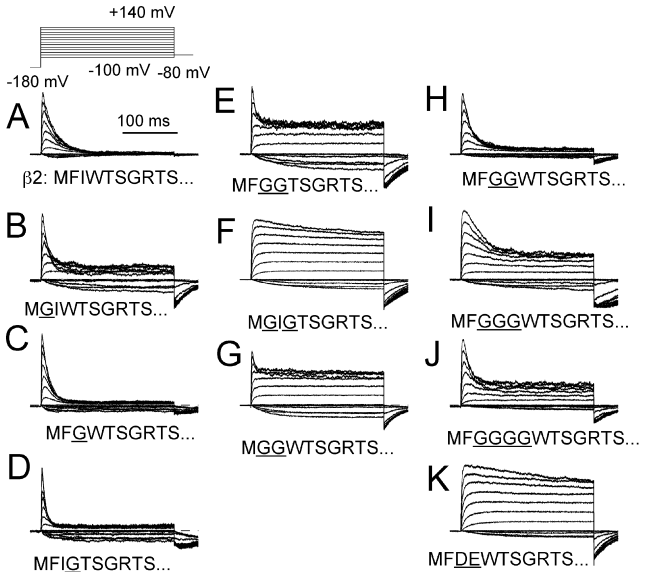

FIGURE 5. Consequences of replacement of one or two residues in the FIW epitope. In A, inactivating currents resulting from wild-type β2 subunits are shown. In B–D, glycine was individually substituted for each residue in the FIW epitope. In each case, this resulted in a small weakening of inactivation, with the strongest effect arising from the F2G substitution. In E–G, two glycines were substituted for a pair of residues in the FIW epitope. In F, replacement of both F and W with G abolished inactivation, while the presence of a single F (E) or W (G) appears sufficient to maintain some fast inactivation. In H–K, the consequences of increasing the separation between F and W are illustrated. In H, the presence of two glycines between F and W results in currents similar to those with an FGW epitope, suggesting that W can still contribute to the stability of the inactivated state when there are two glycines interposed. In I and J, three and four glycines are interposed between F and W, in both cases resulting in currents in which steady-state inactivation is comparable to that resulting from FGG (E). This suggests that, in FGGGW (I) and FGGGGW (J), W may not substantially participate in defining the stability of the inactivated state. In K, the introduction of two negative charges between F and W abolishes inactivation.

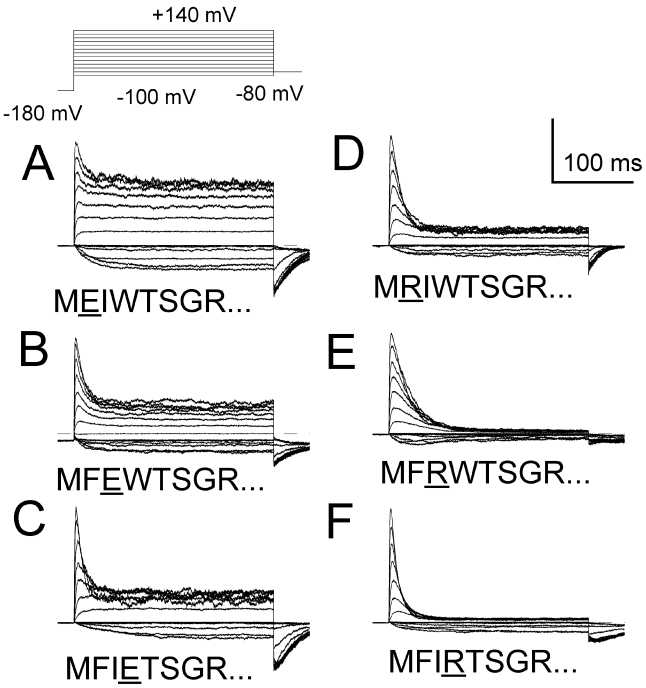

FIGURE 6. Introduction of single charges in the inactivation segment reduces but does not abolish rapid inactivation. In A–C, each residue in the inactivation segment was replaced individually with glutamate. Replacement of F with E (A) produced the most marked disruption of inactivation, with substantial steady-state current observed at all potentials. In D–F, the consequences of replacing each residue with arginine are illustrated. Arginine is less effective in each case at disrupting inactivation than glutamate, although at each position arginine produces some reduction in the stability of the inactivated state. Similar to the action of glutamate, replacement of F with R (D) had the strongest effects in disrupting inactivation. Vertical calibration: A, 4 nA; B, 1.5 nA; C, 5 nA; D, 6 nA; E, 5 nA; F, 4 nA.

the spacer (e.g., FDEW), inactivation is completely lost.

Examples of the consequences of introduction of positive (Arg) or negative (Glu) charge into each of the three positions are provided in Fig. 6. In general, the introduction of a glutamate was more effective at disrupting inactivation than the introduction of an arginine, although in all cases inactivation still occurs. Furthermore, charges in position 2 (F) were more disruptive of inactivation than at positions 3 or 4.

Constructs containing III, WWW, and FFF in the three positions after methionine exhibited some interesting features. In particular, whereas most mutations in the FIW epitope either had minimal effects on τ_{on} or resulted in faster inactivation, WWW was the one construct in which τ_{on} was appreciably slower.

The fact that inactivation still occurs after rather extensive mutagenesis of the FIW segment suggests that a specific structure defined by this triplet of residues is probably not critical to inactivation. Therefore, we also examined three constructs in which the positions of the F, I, and W were rearranged: FWI, IWF, and WIF. In each case, these constructs inactivated similarly to wild-type β2 currents (Table II). τ_{off} was also comparable to the wild-type FIW construct, although recovery from inactivation of construct FWI exhibited two exponential components.

To compare the consequences of alterations in the FIW region, the magnitude of the changes in τ_{off} resulting from each mutation is compared along with the magnitude of the changes in τ_{on} in Fig. 7. In terms of kT units, most mutations generally disrupt τ_{off} more than τ_{on}, consistent with the idea that the major effect of the mutations is to promote faster dissociation of the inactivation domain from its binding site. Changes in

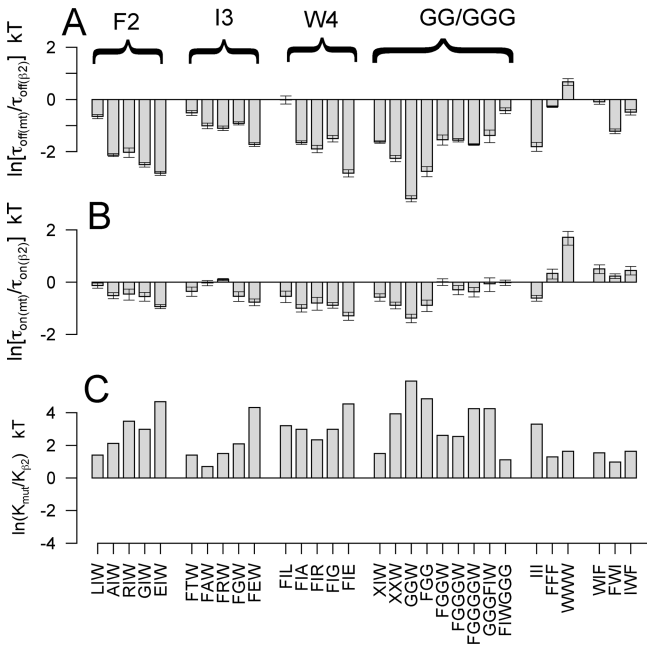

FIGURE 7. Relationship of inactivation parameters to alterations in the FIW triplet. In A, changes in τ_{off} relative to inactivation mediated by wild-type β2 subunits is expressed kT units. Mutations are grouped into those at position 2 (F2), those at position 3 (I3), those at position 4 (W4), constructs with deletions or multiple glycines in the NH_2 terminus, and then a set of repeated residues in the initial triplet (FFF, III, WWW). Error bars reflect standard errors for measurement of the mutant construct expressed relative to the mean β2 estimate. In B, changes in τ_{on} are shown for each construct. Except for the slowing in inactivation resulting from the WWW mutation, most mutations have minimal effects on inactivation onset. In C, effects of mutations are compared in terms of $\ln(K_{mt}/K_{\beta 2})$, which is calculated based on the steady-state current at 100 mV (f_{ss}) and τ_{on} (see MATERIALS AND METHODS).

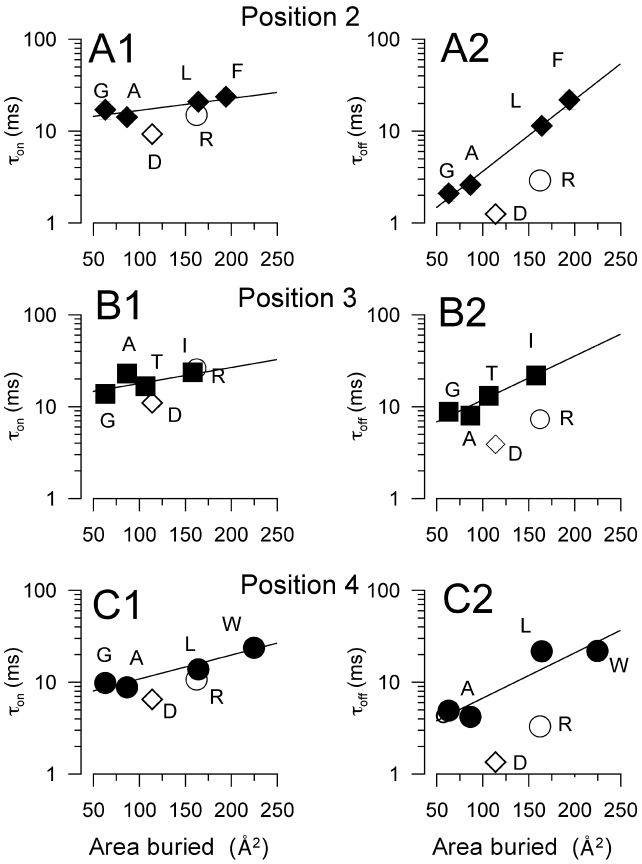

FIGURE 8. Dependence of inactivation onset and recovery on properties of residues in the initial triplet. In A1, τ_{on} (on the left) and τ_{off} (on the right) is plotted as a function of the mean surface area of the residue in position 2 that would be buried on transfer from solvent to a folded protein (Rose et al., 1985). In A2, τ_{off} is plotted as a function of area what would be buried. The lines correspond to linear regressions [τ(area) = B*exp(C*area)] fit through only the uncharged residues. In B1 and B2, τ_{on} and τ_{off} are plotted with respect to area buried on transfer of a residue from solvent to a folded protein in regard to the residue in position 3 in the inactivation epitope. In C1 and C2, τ_{on} and τ_{off} are plotted with respect to area buried on transfer of a residue from solvent to a folded protein in regard to the residue in position 4 in the inactivation epitope.

τ_{on} are much smaller, although not absent. However, for those mutations in which f_{ss} is appreciable, some of the change in τ_{on} may also reflect a small contribution of dissociation to the τ_{on} relaxation. The apparent change in the stability of the inactivated state for each mutant was also plotted in terms of $\ln(K_{mt}/K_{\beta 2})$ (Fig. 7 C), which reflects an apparent affinity calculated from the fraction of steady-state current (f_{ss}) and τ_{on}.

To evaluate the consequences of single point mutations in the FIW segment, τ_{on} and τ_{off} were plotted (Fig. 8) as a function of the mean surface area of the amino acid that is buried upon transfer from a solvent to a folded protein (Rose et al., 1985). This is one of many measures of relative hydrophobicity among amino acids. In all cases, for the uncharged substitutions at each position, $\log(\tau_{off})$ varies in a linear fashion with hydrophobicity (Fig. 8, A2, B2, and C2), while $\log(\tau_{on})$ exhibits only a weak change with hydrophobicity at each position (Fig. 8, A1, B1, and C1). Substitutions of E and R result in τ_{off} values that deviate from the simple relationship exhibited by the uncharged residues. However, a line through the charged residues can be imagined as roughly parallel with that of uncharged residues. Charged residues pose particular problems for any hydrophobicity ranking (Creighton, 1993). Changes in hydrophobicity in positions 2 and 4 have the largest effects on τ_{off}, consistent with earlier suggestions that these positions are more critical in defining the stability of the inactivated state.

We also examined the impact of bulk hydrophobicity when the first three residues after methionine are considered together. As above, the predicted area transferred upon folding into a protein was determined based on the sum of the contributions of amino acids in positions two to four (Rose et al., 1985) for con-

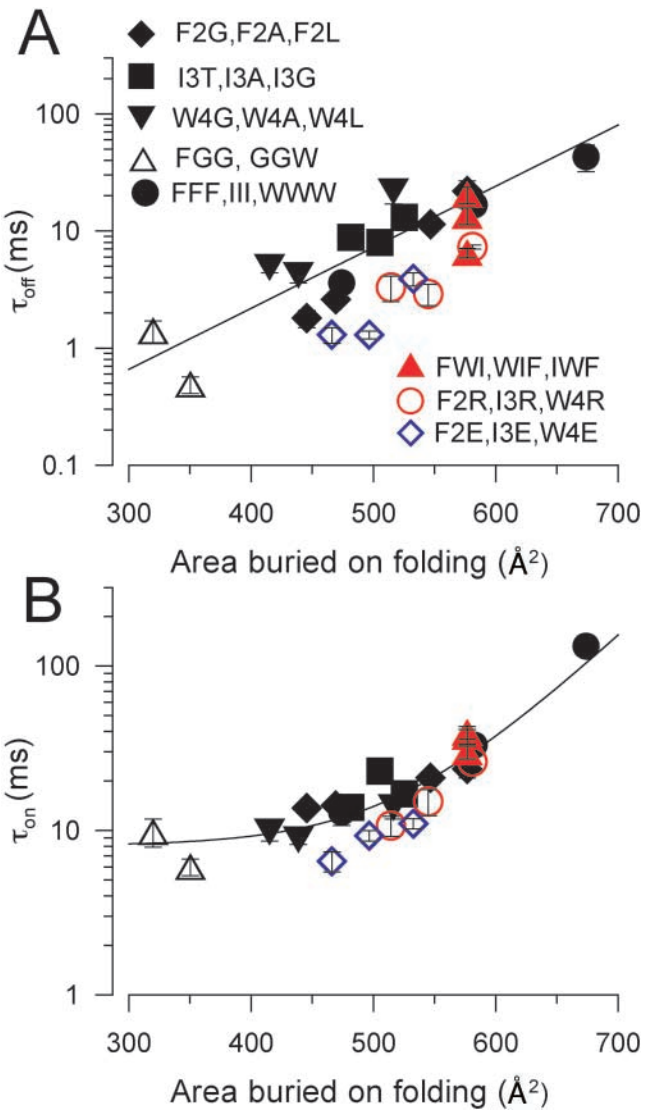

FIGURE 9. Dependence of inactivation parameters on bulk hydrophobicity within the initial triplet. In A, τ_{off} for constructs with mutations within the FIW triplet is plotted as a function of the mean surface area (for the three residues in positions 2–4) that would be buried on transfer from solvent to a folded protein (Rose et al., 1985). The solid line is a linear regression [$\tau_{off}(A) = 0.018 * \exp(0.012*A)$] for all constructs involving uncharged residues. Error bars are SD for a least three determinations. ◆, F2G, F2A, F2L; ■, I3T, I3A, I3G; ▼, W4G, W4A, W4L; △, FGG, GGW; ●, FFF, III, WWW; red ○, F2R, I3R, W4R; blue ◇, F2E, I3E, W4E; red ▲, FWI, WIF, IWF. In B, τ_{on} is plotted as a function of area of residue buried on transfer to a folded protein. Symbols are as in A. The solid line was a fit to constructs with no charges in the initial triplet [$\tau_{on}(A) = 0.002 \exp(0.016A) + 8.0$].

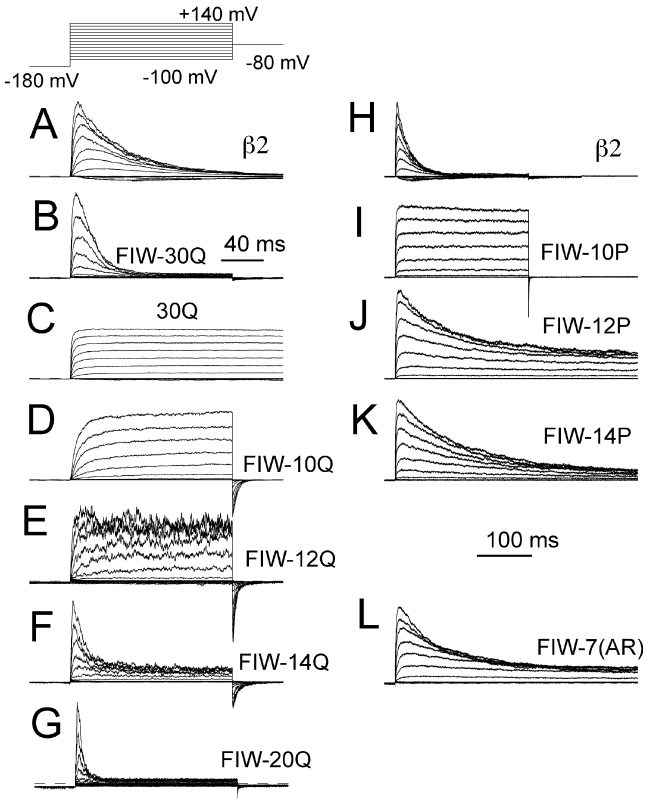

FIGURE 10. NH_2 termini with artificial polymeric linkers support inactivation of BK channels. In A and H, wild-type β2 currents are shown at two different time bases for comparison to mutant constructs. In B, an NH_2 terminus with a polymeric chain length of 30 glutamine residues separating FIW from R46 results in currents that exhibit inactivation. In C, an NH_2 terminus consisting solely of 30 glutamine residues (30Q) does not inactivate. In D, an NH_2 terminus with a polymeric chain length with 10 glutamine residues separating FIW from R46 results in currents that do not inactivate. In E, when the chain length reaches 12 residues, fast time-dependent block is observed at potentials positive to 140 mV, while at more moderate potentials the fast kinetics of block result in an apparent increase in current activation rate. In F and G, traces show inactivating currents resulting from linkers of 14 and 20 glutamine residues, as indicated. In H, wild-type β2 currents are shown on a different time base. In I, the NH_2 terminus contained a linker with 10 proline residues. In J, the linker contained 12 proline residues. In K, the linker contained 14 proline residues. In L, the linker contained 14 residues, an alternating sequence of 7 alanine-arginine pairs.

structs in which changes were only made in the initial triplet. The relationship of this measure of hydrophobicity to τ_{off} and τ_{on} is shown in Fig. 9, A and B, respectively. Similar to the effects of hydrophobicity at the individual positions, $\ln(\tau_{off})$ varies approximately exponentially with hydrophobicity over a rather broad range. Charged residues produce an approximately parallel shift in the relationship between hydrophobicity and $\log(\tau_{off})$. $\log(\tau_{on})$, on the other hand, shows only slight variation with hydrophobicity over a broad range, with slowing in τ_{on} at larger increases in hydrophobicity exemplified by the WWW construct. In contrast to the behavior of $\log(\tau_{off})$, $\log(\tau_{on})$ was better described by a function, including both a hydrophobicity-independent term and a hydrophobicity-dependent term. The dependence of a presumed association rate on an apparent measure of hydrophobicity seems rather surprising, since hydrophobicity would not be

TABLE III

Artificial Linkers Between TM1 and the Inactivation Epitope

Construct	τ_{on} + 100 mV	$\ln(\tau_{on(mut)}/\tau_{on(\beta2)})$	τ_{off} − 140 mV	$\ln(\tau_{off(mut)}/\tau_{off(\beta2)})$	$\ln[K^*_{mt}/K^*_{\beta2}]$	*n*
	ms	*[kT]*	*ms*	*[kT]*	*[kT]*	
β2 (1:1)	23.7 ± 2.9		21.9 ± 4.8			10
FIW-8Q	none		none			3
FIW-9Q	none		none			4
FIW-10Q	none		none			6
FIW-11Q	none		none			6
FIW-12Q	2.6 ± 0.3	−2.210	1.1 ± 0.4	−2.991	0.78	4
FIW-13Q	3.4 ± 0.4	−1.942	0.65 ± 0.08	−3.517	1.58	6
FIW-14Q-	3.8 ± 1.1	−1.830	1.3 ± 0.2	−2.824	0.99	6
FIW-15Q	2.8 ± 0.7	−2.136	2.7 ± 0.7	−2.345	0.21	5
FIW-16Q	3.4 ± 0.7	−1.942	3.2 ± 0.6	−1.923	−0.018	6
FIW-18Q	4.0 ± 0.3	−1.779	5.1 ± 1.0	−1.457	−0.32	6
FIW-20Q	3.4 ± 0.8	−1.942	7.3 ± 1.3	−1.099	−0.84	4
FIW-25Q	5.0 ± 1.6	−1.556	10.1 ± 2.3	−0.774	−0.78	4
FIW-30Q	8.7 ± 0.7	−1.002	11.6 ± 0.5	−0.635	−0.37	4
30Q-R46	none		none			3
FIW-10G-23Q	3.1 ± 0.5	−2.034	4.6 ± 1.0	−1.560	−0.47	3
FIW-12P	141 ± 15	1.783	2.7 ± 0.1	−2.093	3.88	3
FIW-13P	109 ± 21	1.526	5.8 ± 1.4	−1.329	2.86	3
FIW-14P	140 ± 1.6	1.776	21.5 ± 6.2	−0.0184	1.80	3
FIW-7(AR)	111.8 ± 13.5	1.551	4.4 ± 1.1	−1.605	3.16	5

expected to impact on the likelihood of collision in a bimolecular reaction. However, measures of hydrophobicity also tend to be correlated, except in the case of particular polar residues, with the partial volume in solution of a residue. We therefore propose that the slowing of τ_{on} is the result of a steric hindrance that arises from the presence of more bulky residues on the inactivation epitope. We suggest that this reflects movement of the inactivation epitope into a blocking position of somewhat restricted dimension, perhaps the pore.

The Inactivation Epitope (FIW) Is the Necessary and Sufficient Element Required for Inactivation by the β2 Subunit

The results from the deletion mutations suggest that the linker region between FIW and TM1 is relatively unimportant in maintaining the inactivation competency of the β2 NH_2 terminus. In fact, there appears to be little requirement for any specific structure in the linker region, except to provide some minimal length required for the inactivation epitope to reach its site of action. If FIW is the critical epitope required for inactivation while the linker segment is largely irrelevant to the ability of the NH_2 terminus to produce inactivation, artificial NH_2 termini with somewhat arbitrary linkers between TM1 and FIW should also produce inactivation. To evaluate this possibility, an artificial NH_2 terminus was created in which FIW was linked to TM1 by a chain of 30 glutamine residues (polyQ). Residue R46 was maintained in all constructs, since a positively charged residue at this position appears to define the limit of TM1 in all β subunits. Currents arising from an altered β2 construct with an NH_2 terminus consisting of MFIW(30Q)R46-β2 are shown in Fig. 10 B. FIW-30Q exhibited inactivation with both the onset and recovery from inactivation being somewhat faster than for wild-type β2. In contrast, a similar construct with a 30Q NH_2 terminus but no FIW resulted in currents with no inactivation (Fig. 10 C).

A characteristic of inactivation mediated by the β2 NH_2 terminus is that cytosolic blockers do not compete with the inactivation domain for its blocking site (Xia et al., 1999). We were concerned that, with artificial NH_2 termini, the site and mechanism of inactivation might differ from that observed with the wild-type β2 NH_2 terminus. To test this possibility, the ability of QX-314 to compete with inactivation mediated by FIW-30Q was examined. As with the wild-type β2 NH_2 terminus, QX-314 did not hinder the ability of the FIW-30Q NH_2 terminus to produce inactivation (unpublished data).

Polymeric NH_2 Termini Place Constraints on the Distance Between TM1 and the Interaction Site of the Inactivation Epitope

The ability of artificial NH_2 termini to produce inactivation suggests that we can place additional limits on the properties of inactivation-competent NH_2 termini. A series of NH_2 termini with different polyglutamine

(poly-Q) linkers were constructed. At poly-Q lengths of 8, 10 (Fig. 10 D), and 11, no inactivation was observed. In all cases, NH_2 termini with poly-Q lengths from 12 to 30 supported inactivation (Fig. 10, E–G; Table III). At a chain length of 12 residues, direct time-dependent inactivation was observed only at potentials more positive than 140 mV, whereas the low affinity of the inactivation equilibrium and the rapidity of inactivation resulted in currents with a faster apparent activation time course at other potentials (Fig. 10 E). In comparison to the native β2 NH_2 terminus, all constructs with the poly-Q linkers exhibited a faster onset of inactivation and a faster rate of recovery from inactivation, although with longer linker lengths the rates begin to approach those of the wild-type β2 NH_2 terminus. With a linker of 12 residues, the total number of residues from the initiation methionine preceding the R at the beginning of TM1 is 16. It is interesting that noninactivating β1 and β4 NH_2 termini have 14 and 15 cytosolic residues, respectively, suggesting that their terminal residues would rarely approach the position at which the β2 NH_2 terminus acts (Fig. 1 A).

The cut-off of inactivation with a poly-Q linker of less than 12 residues is also generally consistent with the deletion mutations described earlier. In Δ5–24, in which inactivation is preserved (Table I), there are 21 residues between FIW and R46. In contrast, in Δ5–35, there are 10 residues between FIW and R46.

It seems remarkable that a linker as short as 12 residues should support inactivation given that the TM1 of the β2 subunit presumably resides further from the channel axis than the α subunit S0–S6 segments. Can any inferences be made about the length and structure of the peptide segment required for inactivation? Polymeric chains of amino acids are probably best treated as a random coil. In such a case, the rms end-to-end distance for a chain of N residues is given approximately by $\sqrt{130N}$ (Creighton, 1993), such that a chain of 12 residues should, on average, extend ~39.5 Å and a chain of 20 residues, ~51 Å. For comparison, an α-helical coil of 12 residues should extend ~18 Å (1.5 Å/residue) and a β-sheet ~38–40 Å (3.2 Å/residue).

A particularly informative linker would be based on poly-proline (poly-P). Proline adopts neither an α nor β helical shape, but forms its own more rigid helical structures, with a polyproline II conformation (3.33 residues per turn; 3.12 Å per residue) favored in aqueous media (Creighton, 1993). Similar to the poly-Q linkers, a chain of 10 proline residues did not support inactivation, while chains of 12, 13, and 14 residues all supported inactivation (Fig. 10, I–K). Thus, uncharged chains formed by either the rigid proline or the more flexible glutamine exhibit a similar cut-off in terms of the minimum number of residues required to ensure that the inactivation segment reaches a blocking position. For a 12 residue poly-P chain, a polyproline II conformation predicts a length of 37.4 Å. This is remarkably similar to the average end-to-end distance for a random coil, which is likely to apply to the poly-Q chains.

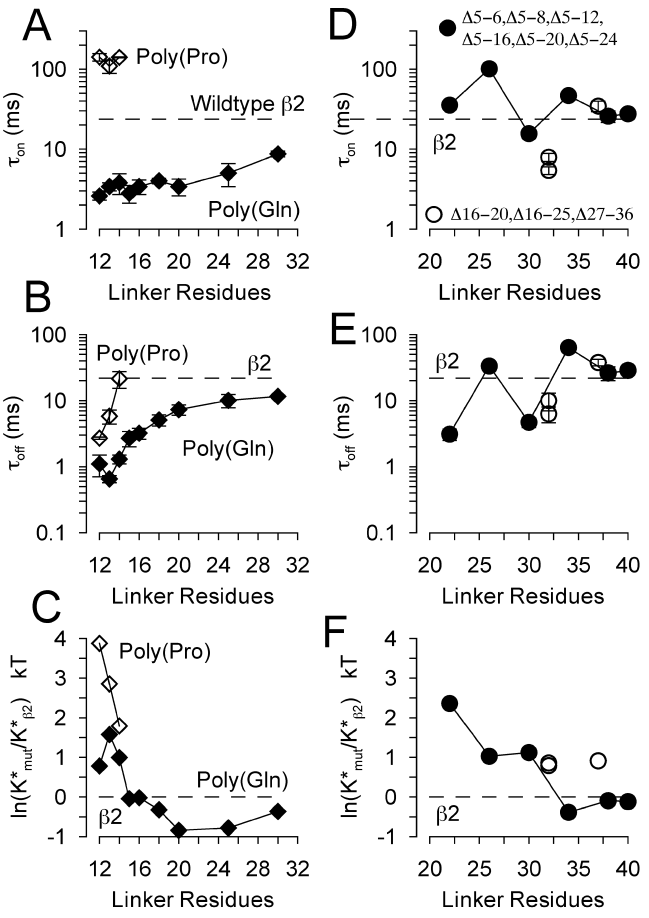

FIGURE 11. Dependence of inactivation properties on lengths of artificial NH_2 termini and altered β2 NH_2 termini. In A, τ_{on} for poly-glutamine (Poly-Q) and poly-proline (poly-P) linkers is plotted as a function of linker length. In B, τ_{off} for poly-Q and poly-P linkers is plotted as a function of linker length. In C, $\ln(K^*_{mt}/K^*_{\beta2})$ is plotted as a function of linker length. In D, τ_{off} is plotted as a function of the length of the β2 NH_2-terminal linker for various deletion constructs, as indicated. In E, τ_{off} is plotted as a function of β2 linker length for various deletion constructs. In F, $\ln(K^*_{mt}/K^*_{\beta2})$ is plotted as a function of linker length for deletion constructs. Dotted lines correspond to values for the wild-type β2 construct.

If the poly-Q linkers adopt a helical structure rather than a random coil, how the FIW inactivation epitope is presented to its interaction site might depend on the fractional rotation of the epitope dependent on the number of turns conferred by different chain lengths. We therefore plotted τ_{on} and τ_{off} as a function of the number of residues in a linker (Fig. 11, A and B). Over a series of poly-Q linkers from 12 through 30 Q, τ_{on} and τ_{off} varied in a continuous fashion, suggesting that the

ability of the FIW epitope to produce inactivation was not particularly constrained by any aspect of the linker.

For both poly-Q and poly-P linkers, τ_{on}, τ_{off}, and $\ln(K^*_{mt}/K^*_{\beta 2})$ (Fig. 11 C) were compared. For poly-Q chains, each parameter varies continuously with chain length approaching values similar to those for the wild-type β2 NH_2 terminus at longer chain lengths. This suggests that, once a particular chain length is reached, the inactivation behavior is largely defined by the inactivation epitope. Although we have not examined longer chain lengths with other amino acids, the limited results with the poly-P linkers also suggest that, as the proline chain length is increased, the inactivation behavior may also begin to approximate that seen with the wild-type NH_2 terminus. An implication of this interpretation is that for shorter chain lengths, the chain is important in defining the ability of the inactivation epitope to reach its site of action.

The differences in the kinetic properties of currents with the poly-P and poly-Q linkers may be explainable in terms of chain flexibility. The poly-Q linker will adopt lengths both shorter and longer than 38 Å and exhibit substantial flexibility, whereas with the more rigid poly-P linker there may be constraints in terms of how the FIW epitope can reach its site of action.

Two other polymeric linkers were also examined. A linker with a series of seven alanine/arginine repeats permitted inactivation (Fig. 10 L). A linker of 14 alanine residues did not result in inactivation. The inability of alanine to support inactivation might result from several reasons. Alanine strongly stabilizes α-helices relative to a random coil arrangement when introduced into artificial peptides (O'Neil and DeGrado, 1990), which might result in a much shorter average length of the alanine chain. However, alanine may also simply prefer a hydrophobic environment, such that the inactivation epitope remains anchored in a position unsuitable for producing inactivation.

For comparison to results with artificial NH_2-terminal linkers, the properties of native NH_2 termini with deletions (Fig. 11, D–F) were also plotted as a function of linker length. For τ_{on} (Fig. 11 D) and τ_{off} (Fig. 11 E), no clear trend with linker length can be discerned, although there is some suggestion, on average, of a faster τ_{off} with shorter chain lengths. However, $\ln[K^*_{mut}/K^*_{\beta 2}]$ (Fig. 11 F) varied qualitatively with chain length in a fashion somewhat similar to that of the poly-Q and poly-P chains with the apparent affinity of the inactivation process reduced at shorter chain lengths.

Mutations that Decrease Net Positive Charge Generally Have Little Effect or Increase the Rate of Current Inactivation

Results above indicate that the necessary elements required to make an inactivation-competent NH_2-terminal segment are a triplet of hydrophobic residues at the NH_2 terminus and a simple linker connecting the FIW triplet to TM1. Yet, in Kv channels charge on the linker is considered to be fundamentally important in the inactivation process, either in guiding interactions of a presumed "ball" domain with a binding site (Murrell-Lagnado and Aldrich, 1993b) or in allowing the inactivation segment to reach its site of action (Zhou et al., 2001). Thus, although uncharged artificial linkers still support inactivation of BK channels, we wished to evaluate whether the natural properties of the β2 linker, e.g., intrinsic structure or the distribution of charged residues, might impact on the inactivation process. Here we examine the consequences of specific alterations in the linker to determine the role of charges or intrinsic structure on inactivation.

Sets of positive charge were neutralized to test for residues important in the inactivation process. Cur-

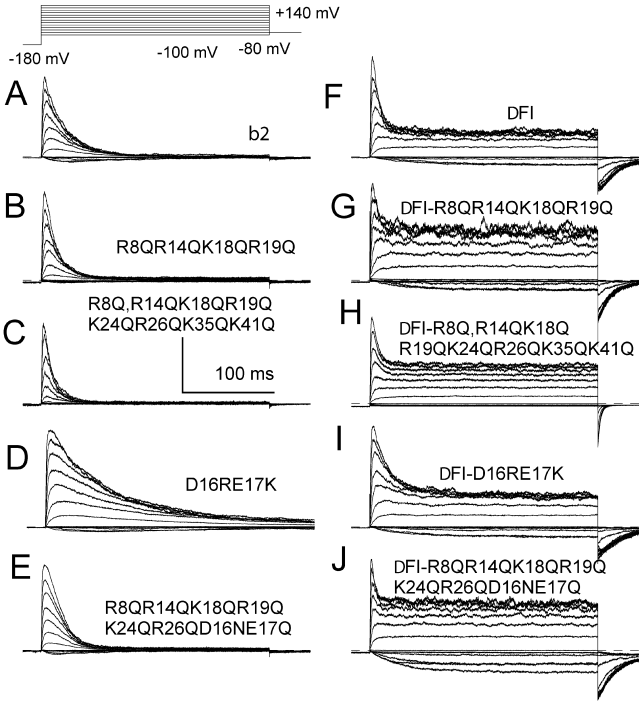

FIGURE 12. Mutations of charged residues have little impact on inactivation mediated by the β2 auxiliary subunit. For A–J, currents were activated by the indicated voltage-protocol, although in D longer activation steps were employed. In A, wild-type β2 currents are illustrated. In B, currents resulted from construct R8QR14QK18QR19Q. In C, currents are from construct R8Q R14QK18QR19QK24QR26QK35QK41Q; in D, D16RE17K; in E, neutralization of all charge in first 26 amino acids, R8QR14QK18QR19QK24QR26QD16NE17Q. In F, currents resulted from a construct with deletion of two of the residues in the inactivation epitope, FI (ΔFI). In G, currents resulted from mutation of R8QR14QK18QR19Q in a background of ΔFI; in H, ΔFI-R8QR14QK18QR19QK24QR26QK35QK41Q; in I, ΔFI-D16RE17K; in J, ΔFI-R8QR14QK18QR19QK24QR26QD16NE17Q. Vertical calibration: A, 3 nA; B, 0.6 nA; C, 1.5 nA; D, 1.5 nA; E, 2 nA; F, 2.5 nA; G, 1.3 nA; H, 5 nA; I, 2.5 nA; J, 1.5 nA.

TABLE IV

Charge Manipulations in the β2 NH_2 Terminus

Construct[1]	τ_{on} + 100 mV	$\ln(\tau_{on(mut)}/\tau_{on(\beta2)})$	τ_{off} − 140 mV	$\ln(\tau_{off(mut)}/\tau_{off(\beta2)})$	$\ln[K^*_{mt}/K^*_{\beta2}]$	*n*
	ms	*[kT]*	*ms*	*[kT]*	*[kT]*	
β2	23.7 ± 2.9		21.9 ± 4.8			10
R8,14K18R19	15.1 ± 0.8	−0.45	12.9 ± 3.9	−0.530	0.079	6
R8,14K18R19K24R26	18.0 ± 2.5	−0.28	13.3 ± 3.0	−0.499	0.22	6
R8,14K18R19K24R26K33R34K41	11.1 ± 0.1	−0.76	4.2 ± 1.6	−1.651	0.89	7
K24R26	22.1 ± 2.6	−0.07	17.2 ± 4.0	−0.242	0.17	6
D16E17	75.5 ± 9.0	1.16	19.7 ± 1.5	−0.106	1.27	4
D27,29,32	53.9 ± 3.9	0.82	24.3 ± 7.9	0.104	0.72	6
D16E17 D27,29,32	234 ± 24	2.29	27.3 ± 5.0	0.220	2.07	7
R8,14K18R19 D16NE17	18.7 ± 2.9	−0.24	15.1 ± 5.5	−0.372	0.14	5
R8,14K18R19K24R26 D16NE17	16.1 ± 2.4	−0.39	8.7 ± 1.5	−0.923	0.54	5
D16R	39.3 ± 4.6	0.51	16.1 ± 1.5	−0.308	0.81	3

Positive charges were changed to Q, unless otherwise indicated. Negative charges were changed to R unless otherwise indicated.

τ_{off} is recovery time constant measured at −140 mV with 10 μM Ca^{2+}; τ_{on} is inactivation time constant measured at 100 mV with 10 μM Ca^{2+}; *n* is the number of patches.

rents resulting from a construct with neutralization of the first four positive charges in the NH_2 terminus (R8QR14QK18QR19Q) are shown in Fig. 12 B. τ_{on} at any voltage is somewhat faster relative to wild-type β2 currents (Fig. 12 A), while the fraction of steady-state current (f_{ss}) is somewhat greater. A number of other constructs with neutralization of positively charged residues also exhibited similar results, with relatively small changes in τ_{on} or f_{ss} (Table IV). The absence of a major role of positively charged residues in the inactivation process is most dramatically illustrated with a construct in which all positive charges up through residue K41 (R8QR14QK18QR19QK24QR26QK33QR34QK35QK41Q) were neutralized. This construct exhibits relatively normal inactivation (Fig. 12 C), although somewhat faster than the wild-type β2 NH_2 terminus. The steady-state level of inactivation was similar in both cases. Clearly, major changes in the overall net charge on the β2 NH_2 terminus do not disrupt the ability of the NH_2 terminus to produce inactivation. Furthermore, τ_{on} and τ_{off} are remarkably unaffected. The changes in the apparent inactivation equilibrium, $\ln[K^*_{mut}/K^*_{\beta2}]$, for all constructs with positive charge neutralizations in the first 30 amino acids (Table IV) were <1 kT unit.

For a few constructs, we observed that the $V_{0.5}$ for activation at 10 μM Ca^{2+} was somewhat shifted to more positive potentials, in some cases being similar to that observed for expression of the *Slo1* α subunits alone. In general, for these constructs, some positively charged residues between position 31 and position 46 were neutralized. These effects will be considered elsewhere. A consequence of a positive shift in activation $V_{0.5}$ is that a faster value for τ_{off} will be measured at −140 mV, because of coupling of the recovery process to activation (Ding and Lingle, 2002). For example, the construct with complete neutralization of positive charge exhibited a $V_{0.5}$ value that was shifted close to that resulting from α alone and τ_{off} in this construct, measured at −140 mV, was 4.2 ± 1.6 ms. Thus, in this case, the apparent change in τ_{off} and, therefore, $\ln(K^*_{mt}/K^*_{\beta2})$ probably arises from factors other than intrinsic aspects of the inactivation process. For most constructs described here, $V_{0.5}$ measured at 10 μM Ca^{2+} was, on average, within ±20 mV of that measured for the wild-type β2 subunit.

Charge Reversals of Negatively Charged Residues Slow the Onset of Inactivation

There are five negative charges in the first 32 amino acids of the β2 NH_2 terminus. In construct D16RE17R, in which this net charge is increased from +2 to +6, τ_{on} is slowed (~75 ms at 100 mV; Fig. 12 D) in comparison to wild-type α + β2 currents, and even with prolonged voltage steps inactivation is less complete (f_{ss} = 0.027) than for wild-type currents. τ_{off} was somewhat faster than that measured for α + β2 currents. In another construct, the three residues D27D29D32 were all mutated to R. In this case, τ_{on} was about twofold slower than for α + β2 currents, being ~54 ms at 100 mV with 10 μM Ca^{2+}. When all five of these negative charges (D16E17D27D29D32) were simultaneously changed to R, inactivation still occurred, but τ_{on} was further slowed to ~250 ms. These results (Table IV) show that a net increase in the total positive charge on the β2 NH_2 terminus seems to slow the inactivation process, although not abolish it, with only minor effects on recovery from inactivation.

We also examined two constructs in which charge neutralization at D16E17 was coupled to neutralization of positive charge. Thus, for construct R8Q14Q

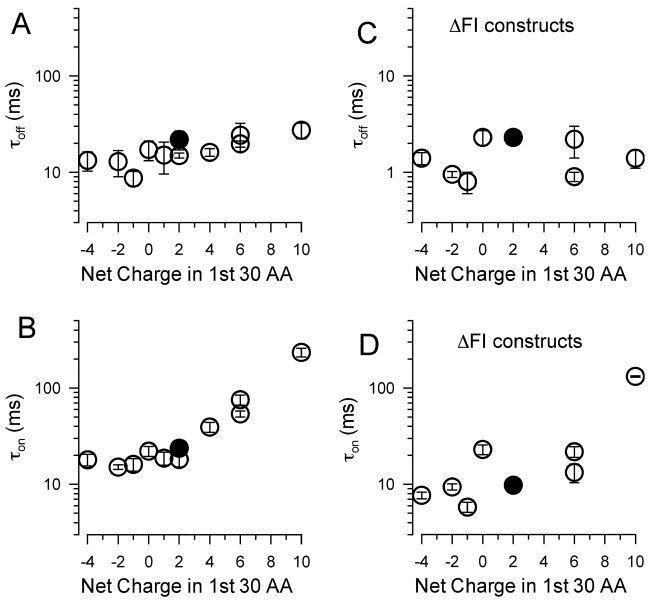

FIGURE 13. Dependence of inactivation properties on net charge in first 30 amino acids of NH_2 terminus. In A, τ_{off} is plotted as a function of net charge in the first 30 amino acids of the NH_2 terminus. Constructs in which residues K33, R34K35, and K41 were mutated were not included in these plots, since shifts in activation $V_{0.5}$ in these constructs resulted in shifts in τ_{off} because of coupling of inactivation to activation. The filled circle corresponds to the wild-type β2 NH_2 terminus. In B, τ_{on} is plotted as a function of net charge. With decreases in net charge, τ_{on} shows little change while increases in net charge result in a slowing of τ_{on}. In C, τ_{off} for constructs with a ΔFI background is plotted as a function of net charge, revealing little dependence of recovery from inactivation on net charge in the linker. In D, τ_{on} is plotted as a function of net charge for constructs with a ΔFI background.

K18QR19QD16NE17Q, all charges in the first 23 amino acids and, for construct R8Q14Q K18QR19QK24QR26QD16NE17Q, all charges in the first 26 amino acids of the NH_2 terminus have been removed. For both cases, currents were remarkably comparable to wild-type α + β2 currents (Fig. 12 E for R8QR14QK18QR19QK24QR26QD16NE17Q) with both τ_{on} and τ_{off} being somewhat more rapid than for α + β2 currents (Table IV). Thus, in the total absence of charge on the first 26 amino acids of the NH_2 terminus, the molecular steps in the inactivation process and the efficacy of the inactivation process are relatively unaffected.

The dependence of τ_{on} and τ_{off} on bulk charge on the first 30 residues of the NH_2 terminus is summarized in Fig. 13, A and B. Recovery from inactivation exhibits a very weak dependence on bulk charge in the NH_2 terminus (Fig. 13 A), while, when net charge begins to exceed 2, the onset of inactivation slows. Qualitatively, these effects of bulk charge on inactivation kinetics are rather minor compared with large changes in the blocking rates of *Shaker* NH_2-terminal peptides, in which reversal of two negative charges in the first 15 amino acids can increase the forward rate of block almost 2 orders of magnitude (Murrell-Lagnado and Aldrich, 1993b). Furthermore, whereas neutralization of 3 positively charged residues in the *Shaker* NH_2 terminus (R17QK18QK19Q) resulted in a 6.6-fold slowing of the inactivation rate (Murrell-Lagnado and Aldrich, 1993b), neutralization of 4 positively charged residues (R9Q,R14Q,K18Q,R19Q) in the BK β2 NH_2 terminus resulted in a 1.6-fold increase in the inactivation rate (Table IV). Thus, the changes in τ_{on} resulting from positive charge neutralization are the opposite of those observed for mutations in the *Shaker*B NH_2 terminus and in *Shaker* peptides.

Electrostatic Interactions also Play Little Role When the Binding Affinity of the Inactivation Epitope Is Reduced

Is it possible that charged residues do play an important role in the inactivation process, but that complexities in the inactivation process obscure the charge dependence? Perhaps in a two-step inactivation process (Scheme II), a binding step involving electrostatic interactions may be masked by a subsequent rate-limiting step in which charge plays little role. To assess this possibility, we studied charge mutations in an NH_2-terminal background in which both residues F2 and I3 were removed: construct ΔFI. Because of the appreciable steady-state current (f_{ss}) in this construct (Fig. 12 F), electrostatic interactions that may be critical to the inactivation process may be revealed in this construct. Therefore, charged residues in the ΔFI background were altered to mirror constructs already described (Fig. 12, B–E). In general, the effects of charge alterations for all such ΔFI constructs (Fig. 12, G–J) produced effects that were qualitatively similar to charge manipulations in the wild-type β2 constructs. Neutralization of positively charged residues resulted in only small changes in τ_{on}, as illustrated for ΔFI-R8QR14QK18QR19Q (Fig. 12 G) and for ΔFI-R8QR14QK18QR19QK24QR26QK33QR34QK35QK41Q (Fig. 12 H). Reversal of negative charge in the ΔFI background also resulted in changes in inactivation behavior similar to the same mutations with a full FIW epitope. For example, D16RE17R in the ΔFI background resulted in a slower inactivation time course (Fig. 12 I), similar to the effects of this mutation with an intact inactivation epitope. Also, neutralization of all charges in the first 26 amino acids within the ΔFI background resulted in currents with properties rather similar to those observed with ΔFI (Fig. 12 J, Table IV).

The dependence of τ_{on} and τ_{off} on net charge in the first 30 NH_2-terminal residues in the ΔFI background is summarized in Fig. 13, C–D. As for channels with a normal FIW NH_2 terminus, τ_{off} exhibits little dependence on bulk charge in the NH_2 terminus (Fig. 13 A),

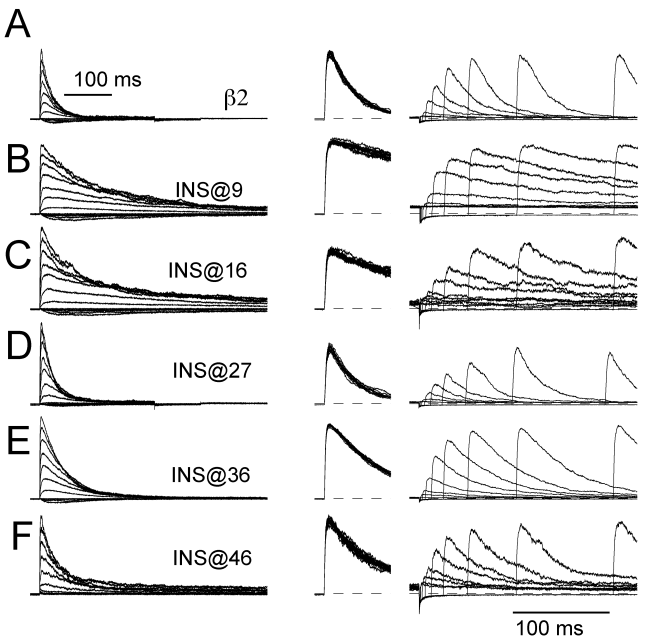

FIGURE 14. Effects of insertions in the β2 NH_2 terminus. A fourteen residue insert (6QSG6Q) was introduced into the β2 NH_2 terminus beginning at positions 9, 16, 27, 36, and 46. In A, inactivation onset for wild-type β2 currents is shown on the left for activation potentials from −100 through 140 mV. On the right, wild-type β2 currents resulting from a paired pulse protocol to define the time course of recovery from inactivation are shown. The duration of the initial inactivation pulse varied for different constructs to ensure that inactivation was essentially complete before the onset of a recovery interval (τ_{on} ~22 ms; τ_{off} ~24 ms). In B, inactivation onset (on the left) and recovery from inactivation for an NH_2 terminus with the 14 amino acid insert at position 9 (INS@9) are shown. Inactivation onset is slowed about fourfold (τ_{on} ~183 ms), while recovery from inactivation (τ_{off} ~34 ms) is only slightly affected. In C, currents resulted from an NH_2 terminus with the insert at position 16 (INS@16). Both inactivation onset (τ_{on} ~174 ms) and recovery (τ_{off} ~36.7 ms) are slowed relative to wild-type currents. In D, currents resulted from an insert at position 27 (INS@27), with both the onset (τ_{on} ~26.2 ms) and recovery (τ_{off} ~31 ms) from inactivation being similar to wild-type currents. In E, in construct INS@36, onset (τ_{on} ~52 ms) and recovery (τ_{off} ~17 ms) from inactivation are similar to wild-type currents. In F, in construct INS@46, a shift in the $V_{0.5}$ of activation is observed, along with an increase in recovery rate (τ_{on} ~49 ms; τ_{off} ~13.4 ms).

whereas, when net charge begins to be large, τ_{on} slows. Qualitatively, these results differ markedly from those obtained for charge mutations in the *Shaker*B NH_2 terminus (Murrell-Lagnado and Aldrich, 1993b).

Effects of Insertions in the β2 NH_2 Terminus

Another approach to examination of the potential structural constraints imposed by the NH_2 terminus is to examine the consequence of insertions at different positions in the NH_2 terminus. We therefore created a series of constructs in which a chain of 14 amino acids (6Q-SG-6Q) was inserted at various positions in the β2 NH_2 terminus (Table VI). Irrespective of whether the insert was at position 9, 16, 27, 36, or 46, inactivation remained intact (Fig. 14, B–F). With insertion near the key inactivation epitope (at positions 9 or 16), τ_{on} was slowed, while τ_{off} was relatively unaffected. In another construct, 15Q was used to replace residues 26–45. This construct behaved in a fashion similar to the native β2 NH_2 terminus. These results further support the general idea that residues from position 5 through position 35 have little specific role in defining the properties of inactivation. Although the exact rates of inactivation onset and recovery exhibit variability among constructs, the key point is that essentially complete inactivation still occurs and that the apparent stability of the inactivation process is little affected by manipulations of the linker (Tables IV–VI).

Point Mutations at Other Positions in the β2 NH_2 Terminus Have Little Effect on Inactivation

We also mutated other residues over much of the NH_2 terminus, attempting to make changes that altered some key physicochemical property of the amino acid at a given position. These results are summarized in Table VII. As with the charge mutants, inactivation remains relatively unaltered over all positions examined, with only relatively small changes in inactivation onset or recovery.

DISCUSSION

The results presented here provide a compelling picture of the essential elements required to form a β subunit inactivation-competent NH_2 terminus. Inactivation occurs when a set of 1 to 3 sufficiently hydrophobic and large residues is linked to the first TM segment by a minimum of 12 amino acids of any of a variety of sequences, including both charged or neutral linkers. These simple requirements are quite remarkable, since they strongly suggest that a specific structure of the NH_2 terminus is not required. Rather, as discussed below, the results suggest that insertion of the appropriate hydrophobic residues into the permeation pathway is the key step leading to producing inactivation. These results are of general interest to Kv channels, since the BK β2 subunit shares two common features with virtually all inactivating NH_2 termini of voltage-dependent K^+ channel α and β subunits. First, there is usually a set of hydrophobic residues at the beginning of the NH_2 terminus and, second, the sequence after the hydrophobic residues is usually rich in charged residues. To what extent then is the rapid inactivation mechanism of Kv channels similar to that of BK channels?

TABLE V

Charge Alterations in a Background of a ΔFI Deletion

Construct	τ_{on} + 100 mV	$\ln(\tau_{on(mt)}/\tau_{on(\Delta FI)})$	τ_{off} − 140 mV	$\ln(\tau_{off(mt)}/\tau_{off(\Delta FI)})$	$\ln[K^*_{mut}/K^*_{\beta 2}]$	f_{ss}	$\ln[K_{mt}/K_{\beta 2}]$	*n*
	ms	*[kT]*	*ms*	*[kT]*	*[kT]*		*[kT]*	
β2	23.7 ± 2.9	0.88	21.9 ± 4.8	2.25	−1.37	0.005	−3.93	10
ΔFI	9.8 ± 1.2	—	2.3 ± 0.3	—	—	0.204	—	8
ΔFI-R8,R14	23.0 ± 2.7	0.853	2.3 ± 0.4	0	0.85	0.47	1.24	5
ΔFI- R8,R14,K18,R19	9.4 ± 0.7	−0.0417	0.95 ± 0.07	−0.884	0.84	0.53	1.48	6
ΔFI-R8,R14,K18,R19,K24,R26,D16N,E17Q	5.8 ± 0.7	−0.525	0.8 ± 0.2	−1.056	0.53	0.48	1.28	4
ΔFI-R14,K18,R19,K24,R26,K33,R34,K35,K41	7.7 ± 0.6	−0.241	1.4 ± 0.2	−0.496	0.26	0.35	0.74	4
ΔFI-D16R,E17K	21.8 ± 2.8	0.800	2.2 ± 0.8	−0.044	0.84	0.43	1.08	6
ΔFI-D27R,D29R,D32R	13.3 ± 2.9 (+140 mV)	0.305	0.9 ± 0.1	−0.938	1.24	0.72	2.31	6
ΔFI-D16R,E17K D27R,D29R,D32R	132 ± 21	2.600	1.4 ± 0.3	−0.496	3.10	0.61	1.81	4

Do Kv and BK Channels Share a Similar Inactivation Mechanism?

Despite the shared structural elements between Kv and β2 inactivation domains, there are functional differences in the inactivation mechanisms between both that have raised the possibility that the underlying molecular mechanisms may differ in important ways. For example, in contrast to Kv channels, cytosolic blockers do not impede movement of the β2 inactivation epitope into its blocking position (Solaro et al., 1997; Xia et al., 1999, 2000). Also in contrast to Kv inactivation, the BK inactivation epitope blocks in a position that does not impede channel closure upon repolarization (Solaro et al., 1997). Although such results raise the possibility that inactivation of BK channels occurs at a site outside the channel pore, the fact that each inactivating NH_2 terminus acts independently to produce inactivation (Ding et al., 1998; Xia et al., 1999) and that recovery from inactivation involves dissociation of a single inactivation particle (Ding et al., 1998) is most easily explained by the idea that the likely site of action of any inactivation particle is on the axis of the permeation pathway.

The structural picture of Kv channel inactivation advanced considerably with the demonstration that the terminal residues of the Kvβ2 NH_2 terminus specifically interact with pore-lining residues of the Kv1.4 α subunit (Zhou et al., 2001). Our demonstration that inactivation of BK channels depends on a critical initial segment of residues in the NH_2 terminus fits very nicely with this picture of Kv inactivation, in which the blocking particle is a linear peptide segment that inserts into the ion permeation pathway (Zhou et al., 2001). Furthermore, as discussed below, the tolerance of the inactivation segment to rather extensive mutagenesis would seem generally consistent with the rather nonselective mechanism implied by simple insertion of a peptide into the permeation pathway. How then can the differences between Kv and BK inactivation be explained?

To reconcile the apparent differences between Kv and BK inactivation, we suggest that inactivation of BK channels occurs through interaction of the NH_2-terminal peptide segment with a site in the permeation pathway that precedes the deactivation gate. Thus, the actual site of interaction of FIW residues may be at some distance from the deactivation gate, at a position within the entryway to the pore and relatively distant from the binding sites for cytosolic blockers. Although the wide entryway described for the open state of one bacterial

TABLE VI

Insertions and Replacements in the β2 NH_2 Terminus

Construct	τ_{on}	$\ln(\tau_{on(mut)}/\tau_{on(\beta 2)})$	τ_{off}	$\ln(\tau_{off(mut)}/\tau_{off(\beta 2)})$	$\ln[K^*_{mt}/K^*_{\beta 2}]$	f_{ss}	$\ln[K_{mt}/K_{\beta 2}]$	*n*	Len
	ms	*[kT]*	*ms*	*[kT]*	*[kT]*		*[kT]*		
β2 (1:1)	23.7 ± 2.9	—	21.9 ± 4.8	—	—	0.005	—	10	42
INS@9	200 ± 23	2.133	25.0 ± 7.9	0.132	2.00	0.045	2.24	5	56
INS@16	177 ± 18	2.011	35.3 ± 8.1	0.477	1.53	0.1	3.10	5	56
INS@27	32.5 ± 5.3	0.317	25.7 ± 6.7	0.160	0.16	0.020	1.40	7	56
INS@36	55.3 ± 2.6	0.847	17.0 ± 2.0	−0.253	1.10	0.005	0.00	3	56
INS@46	55.3 ± 7.3	0.847	12.8 ± 3.3	−0.537	1.38	0.09	2.98	4	56
Δ26-45/15Q	14.2 ± 1.8	−0.512	15.8 ± 3.1	−0.326	−0.19	0.003	0.51	4	37

For each Ins@# construct, 14 residues (QQQQQQSGQQQQQQ) were inserted at the indicated position. Len, number of residues between FIW and R46.

TABLE VII

Miscellaneous Mutations in the First 31 Amino Acids of the β2 NH_2 Terminus

Construct	τ_{on} + 100 mV	$\ln(\tau_{on(mut)}/\tau_{on(\beta2)})$	τ_{off} − 140 mV	$\ln(\tau_{off(mut)}/\tau_{off(\beta2)})$	$\ln[K^*_{mt}/K^*_{\beta2}]$	*n*
	ms	*[kT]*	*ms*	*[kT]*	*[kT]*	
β2 (1:1)	23.7 ± 2.9	—	21.9 ± 4.8	—	0	10
T5N	22.3 ± 2.8	−0.0609	11.4 ± 1.2	−0.652	0.59	7
S6N	32.0 ± 5.5	0.300	8.6 ± 3.7	−0.935	1.24	4
G7P	30.7 ± 1.1	0.259	43.7 ± 4.2	0.691	−0.43	4
T9N	38.7 ± 3.6	0.490	6.5 ± 1.0	−1.215	1.71	7
T5NS6NT9N	36.0 ± 5.5	0.418	29.3 ± 2.3	0.291	0.13	4
S10N	25.5 ± 0.7	0.0732	23.5 ± 6.2	0.0705	0.0027	5
S11N	25.0 ± 2.4	0.0534	16.6 ± 5.1	−0.277	0.33	4
S12N	28 ± 2.0	0.167	22.2 ± 3.2	0.0136	0.15	4
Y13N	22.5 ± 2.6	−0.0520	34.4 ± 7.4	0.452	−0.50	6
Y13T	28.5 ± 2.9	0.184	19.2 ± 2.0	−0.132	0.32	4
H15L	23.9 ± 3.4	0.008	33.8 ± 5.8	0.434	−0.43	3
N20I	25.4 ± 3.0	0.0693	20.1 ± 7.3	−0.0858	0.16	3
I21Y	18.2 ± 1.8	−0.264	26.3 ± 7.0	0.183	−0.45	3
Y22N	20.8 ± 2.9	−0.131	40.3 ± 6.4	0.610	−0.74	4
Q23L	20.0 ± 3.0	−0.170	21.0 ± 2.0	−0.0420	−0.13	4
I25Y	14.8 ± 1.5	−0.471	31.0 ± 6.2	0.348	−0.82	3
H28L	32.3 ± 3.1	0.310	10.4 ± 1.6	−0.745	1.05	6
L30YL31Y	17.4 ± 2.3	−0.309	24.1 ± 9.9	0.0957	−0.41	4

K^+ channel might seem to argue against this possibility (Jiang et al., 2002), the presence of proline and glycine residues at various positions both in Kv and *Slo1* α subunits may result in open state topologies that differ quite dramatically among different channels. At present, there is no information about the topology of the cytosolic side of the BK ion permeation pathway. Whereas Kv channels share two proline residues near the position of a proposed deactivation gate (del Camino and Yellen, 2001), the *slo1* α subunit contains only a single homologous proline. Thus, differences may exist in the topology of inner helices and the ion permeation pathway between these two types of K^+ channels, perhaps resulting in differences in the positions at which inactivation segments might occlude permeation.

From the perspective that the mechanism of rapid inactivation of Kv and BK channels is likely to be generally similar, albeit with some differences in detail, the rest of this DISCUSSION will therefore consider the implications of our results within the context of this type of inactivation mechanism. Furthermore, the extent to which rapid inactivation of all Kv channels can be accounted for by a peptide insertion mechanism will be considered.

Consequences of Deletions within an Inactivating NH_2 Terminus

The consequences of deletions within the β2 NH_2 terminus seem most easily interpretable in terms of the simple picture of inactivation presented above. First, residues from positions 5 through 36 contribute minimally either to the onset or stability of the inactivated condition. Second, deletions of the initial triplet after methionine abolish inactivation. Thus, any structure defined by residues 5–36 seem relatively unimportant and the simplest explanation for the role of the FIW residues would seem to be that it simply inserts into the ion permeation pathway as proposed for inactivation of Kv1.4 (Zhou et al., 2001).

Deletion constructs have also been used to study inactivation mediated by two other Kv NH_2 termini. Can this idea that inactivation results from linear entry of the initial peptide segment into the channel account for inactivation by other Kv NH_2 termini? For the *Shaker*B K^+ channel (Hoshi et al., 1990; Zagotta et al., 1990; Murrell-Lagnado and Aldrich, 1993a,b), it has been shown that, of a series of deletions spanning position 6 through 60, only deletions that included residues within the initial 20 residues abolish inactivation (Hoshi et al., 1990). The consequences of some deletions and mutations in the *Shaker*B NH_2 terminus are summarized in Table VIII. The smallest deletion that removed inactivation was Δ6–9. Deletion of residues in positions 2–5 was not reported, so direct comparison to the present results is not possible. The ability of the Δ6–9 deletion to abolish inactivation might seem to differ from the idea that the initial NH_2-terminal residues are critical. Furthermore, the fact that two nonoverlapping segments of the NH_2 terminus, Δ6–9 and Δ14–40, both abolish inactivation would seem at variance with

TABLE VIII

ShakerB NH_2-terminal Deletion Constructs (Hoshi et al., 1990)

Construct	Sequence of first 20 residues	Net charge	Inactivation
*Shaker*B	MAAVAGLYGL GEDRQHRKKQ...	+2	+++
Δ6–9	MAAVALGEDR QHRKKQQQQQ...	+2	—
L7E	MAAVAGEYGL GEDRQHRKKQ...	+1	—
L7K	MAAVAGKYGL GEDRQHRKKQ...	+3	—
Δ6–29	MAAVAQLEQK EEQKKIAEAK...	0	—
Δ6–46	MAVVALREQQ LQRNSLDGVY...	+1	—
Δ6–60	MAVVAGSLPK LSSQDEEGGA...	−2	—
Δ23–37	same as wild-type	+2	+++
Δ14–40	MAVVAGLYGL GEDRAEAKLQL	−1	—

the idea that only entry of the initial residues is important. However, there are alternative explanations of the various deletion results that may support the idea that common mechanism is involved.

Deletions within an inactivating NH_2 terminus might disrupt inactivation in at least three ways. First, deletions may remove a key set of residues that actually mediate binding of the NH_2 terminus. Second, deletions may cause a structural change in the NH_2 terminus that alters the availability of the binding domain to reach its blocking site. Third, the deletion may promote downstream residues into a position that now obstructs inactivation mediated by other residues.

In the case of *Shaker*B inactivation, for deletions near the NH_2 terminus, the consequences of promotion of downstream residues into the initial 10 residues may have functional consequences unrelated to the residues directly involved in binding. For example, for the Δ6–9 construct, positions 8–10 are all charged residues. Introduction of positive charge at positions 8 and 10 in *Sh*B NH_2-terminal peptides increases the off-rate of peptide block (Murrell-Lagnado and Aldrich, 1993b). Thus, the absence of inactivation in the Δ6–9 construct may reflect, not simply the loss of residues involved in binding, but the de novo presence of charge sufficiently close to the initial hydrophobic residues (MAAVAGLY) that may destabilize binding within the pore. Similar arguments can be made to explain results with other deletion constructs. However, these considerations do not diminish the key conclusion that hydrophobic residues over positions 4–10 in the *Shaker*B NH_2 terminus are clearly important to inactivation (Hoshi et al., 1990; Murrell-Lagnado and Aldrich, 1993b). An explanation for the *Shaker*B deletion Δ14–40 is less obvious, but may simply reflect the fact that, perhaps for *Shaker*, some net positive charge on the first 20 residues of the NH_2 terminus is required to ensure a sufficiently rapid movement of the NH_2 terminus to its blocking site. Thus, although this issue is not proven, it remains possible that linear entry of the initial residues of the *Shaker*B NH_2 terminus into the permeation pathway may also be characteristic of this channel, with perhaps the smaller residues at the end of the ShakerB NH_2 terminus (MAAVAG) allowing deeper entry of the NH_2 terminus into the central cavity, such that residues in positions 6–9 are more important in defining the stability of the inactivated state.

Another interesting case concerns the "secondary" inactivation site that is revealed after deletion of residues 2–39 in Kv1.4 (Kondoh et al., 1997; Hollerer-Beitz et al., 1999). If the primary requirement for an inactivation-competent NH_2 terminus is a sufficiently hydrophobic segment of residues at the NH_2 terminus, it would appear that deletion of residues 2–39 in Kv1.4 (Kv1.4Δ2–39; Fig. 1 B) may simply have resulted in the promotion of another set of appropriately hydrophobic residues into the position that allows its insertion into the ion permeation pathway.

Diversity Among Inactivating NH_2 Termini

The idea that inactivation may result from insertion into the ion permeation of a rather nonspecific set of sufficiently hydrophobic residues may help explain the large diversity in sequences among inactivating NH_2 termini of both α and β subunits (Fig. 1 B) (Hoshi et al., 1990; Ruppersberg et al., 1991; Murrell-Lagnado and Aldrich, 1993b; Tseng-Crank et al., 1993; Rasmusson et al., 1997). An alternative explanation would be that, in each ion channel, the binding site is sufficiently dissimilar that different NH_2-terminal sequences are required. However, three factors suggest that well-defined differences in binding sites may not explain the variations in NH_2-terminal structures. First, isolated NH_2-terminal peptides appear to exhibit considerable promiscuity in their blocking effects on different ion channels, suggesting that the elements required for peptide blockade are shared among channels. Thus, the *Shaker*B ball peptide has been shown to block not only *Shaker* channels, but KV1.4, BK channels (Foster et al., 1992; Solaro and Lingle, 1992; Toro et al., 1992), and cyclic nucleotide–gated channels (Kramer et al., 1994). Second, inactivation domains can tolerate rather extensive mutagenesis with only rather minor changes in the ability of the structure to produce inactivation (Hoshi et al., 1990; Murrell-Lagnado and Aldrich, 1993b). Third, although some NH_2-terminal inactivation domains appear to exhibit well-ordered features when examined by NMR (Antz et al., 1997), in solution most inactivation domains appear to be rather disordered right at the NH_2 terminus, including *Shaker* (Schott et al., 1998), KV1.4 (Antz et al., 1997), KVβ1.1 (Wissmann et al., 1999), and the BK β2 NH_2 terminus (Bentrop et al., 2001).

Given the idea that inactivating NH_2 termini may snake into the ion permeation pathway (Zhou et al., 2001), two primary factors would contribute to the abil-

ity of the NH_2 termini to block the channel: hydrophobicity and steric factors. Favored residues would simply be those that most effectively minimized occupancy of the pore by salts and water, while being of a size suitable to enter the dimensions of the pathway. Based on this idea, NH_2-terminal sequences would probably tolerate a variety of mutations with minimal disruption of the basic inactivation phenomenon, large variation in the sequences of inactivation-competent NH_2 termini would be tolerated, and the absence of a well-defined solution structure would not be unexpected. Thus, the idea of peptide segment insertion into a channel seems more congruent with the set of available information than the alternative view that each inactivation domain (ball) defines a very specific structure that blocks by interaction with a specific binding site.

The Role of the Initial Three Residues Forming the Peptide Inactivation Segment

A set of three amino acids at the NH_2 terminus of the β2 subunit is the key element defining the apparent efficacy of the native β2-mediated inactivation process. The property of these residues that is most critical to their ability to promote inactivation is bulk hydrophobicity. Thus, the stability of the inactivated state as indicated by the time course of recovery from inactivation [$\log(\tau_{off})$] scaled relatively linearly with hydrophobicity over a range of mutations within the first three positions. Remarkably, the introduction of either a single positive or negative charge in this segment, although decreasing the stability of the inactivated state, does not abolish it.

An interesting aspect of the results was that τ_{on} also exhibited some dependence on hydrophobicity. Since τ_{on} presumably reflects something about the rate of association of the NH_2 terminus with its blocking site, an effect of hydrophobicity is not expected. To explain this observation, we propose that the apparent effect of hydrophobicity reflects a slowing of τ_{on} that occurs with bulkier residues in positions 2–4 of the NH_2 terminus. Thus, bulkier residues may result in steric constraints that limit the rate at which the NH_2 terminus can reach a blocking position. In fact, amino acid hydrophobicity is, to some extent, correlated with the total surface area of a residue in solution (Creighton, 1993), simply because size is in most cases associated with the average surface area of the residue that becomes buried upon folding within a protein (Rose et al., 1985). Thus, if occupancy of a position within the pore underlies inactivation, two properties of a residue may be critical for defining its role in inactivation: first, its ability to reach a particular position and, second, its ability to be accommodated within the hydrophobic lining of the entryway to the pore. Although phenylalanine and tryptophan are considered strongly hydrophobic on most scales (Creighton, 1993), the specific volume in solution is also relatively high for both residues. Thus, in accordance with the idea that an initial inactivation segment must snake its way a relatively narrow entryway to the ion permeation pathway, the stability of the interaction of a blocking epitope with the channel may also depend on steric factors related to how the volume of critical residues occupies the permeation pathway. Once within the permeation pathway, smaller residues will simply allow more degrees of freedom of movement, perhaps less effectively excluding water from the space occupied by the blocking epitope. Larger residues will slow movement of the inactivation segment to its blocking site. The slower forward rate of inactivation of the WWW NH_2 terminus may reflect this idea.

The Role of Structure and Charge in the Linker

Another remarkable feature of the present results was that neither any particular structure or charge distribution seems to be particularly important for the inactivation process. We employed both deletions and insertions to disrupt the structure of the linker. Although both deletion mutations and insertions have some effects on the onset and recovery from inactivation, on balance these effects are rather minor, suggesting that a specific structure in the β2 NH_2 terminus is not critical to the ability of the NH_2 terminus to mediate inactivation.

Yet, it should be noted that some deletion and insertion constructs did produce some alteration of inactivation. For example, of the deletion and insertion mutations, constructs Δ5–20, Δ5–24, INS@9, and INS@16 resulted in the greatest disruption of inactivation. An NMR study of the β2 NH_2-terminal peptide has suggested that two segments of the NH_2 terminus adopt a helical structure, residues 11–17 and residues 20–30 (Bentrop et al., 2001). In the proposed structure, the junction between the two relatively well-defined segments exhibits a bend, while residues 1–10 and those following after 32 do not appear to adopt any defined structure. It is possible that the insertion and deletion constructs with the strongest effects may have impacted on the relative positioning of the two relatively well-defined segments observed in the NMR structure. Thus, the specific structure of the β2 NH_2 terminus may influence the rates at which the FIW segment move into and out of its position of block. Yet, the primary conclusion remains that any intrinsic structure in the β2 NH_2 terminus is not critical to the ability of the NH_2 terminus to produce inactivation.

Another obvious feature of the β2 linker is the abundance of charged residues throughout much of the NH_2 terminus. Extensive manipulations of the charged residues on the NH_2 terminus also indicated that charge on the linker was not particularly critical to

maintaining the inactivation mechanism. This is particularly surprising given the apparent importance of electrostatic interactions in blockade of the *Shaker*B channel by isolated *Shaker*B NH_2-terminal peptides (Murrell-Lagnado and Aldrich, 1993b). In general, positive charge neutralization greatly reduces the forward rate of peptide binding, while increasing net positive charge increases the rate of peptide block.

In light of the results with the *Shaker* peptides, the lack of effect of large changes in net charge on the β2 NH_2 terminus is remarkable. Furthermore, the slowing of β2 inactivation with increases in positive charge are opposite to the effect observed for *Shaker* peptides. Since, as discussed in MATERIALS AND METHODS, it is not possible to relate the present observations to specific molecular rate constants, the significance of the effects of charge mutations remains speculative. However, given that charge mutations have similar effects both with the native FIW inactivation epitope and with the ΔFI NH_2 terminus, it seems safe to conclude that electrostatic interactions are not particularly important in the β2 inactivation mechanism. Furthermore, in the total absence of charge in the first 28 amino acids of the NH_2 terminus, relatively normal inactivation still occurs. Thus, charge per se does not seem to be required for any key steps in the activation process.

What then is the role of charge on the linker and what are the reasons a net increase in positive charge slows inactivation? Here we draw attention to two possibilities that may guide future investigation. First, the linker may play some role in maintaining the NH_2 terminus in a relatively mobile condition that permits movement to its blocking position. In a resting condition, the hydrophobic residues at the NH_2 terminus might tend to interact with numerous other hydrophobic pockets. However, with both positive and negative charges, much of the linker would prefer a strongly hydrophilic environment, perhaps ensuring the availability of the hydrophobic inactivation segment for subsequent blocking steps. All the mutations of charged residues that we have examined involved either charge reversals or neutralization with rather hydrophilic residues. Thus, substitution with glutamine, for example, may ensure sufficient mobility in an aqueous medium to maintain the inactivation process. In contrast, an artificial linker containing 14 alanine residues did not inactivate. Second, the sequence of residues following the S6 segment in the *Slo1* α subunit contains an abundance of positive charge, in contrast to an excess of negative charge after S6 in *Shaker*B. We consider it an intriguing possibility that the slowing in τ_{on} seen with increases in net positive charge may reflect an interaction between the net positive charge on the NH_2 terminus and positive charge on residues following S6. The progressive reversal of charges first at positions E16D17 and then at D27D29D32 results in a relatively monotonic slowing of τ_{on}, suggesting that bulk charge is the primary determinant of the slowing. Perhaps this increase in net positive charge slows the rate of movement of the NH_2 terminus into the pore of the channel through interaction with the charged residues that follow the S6 segment.

The Length of the Linker

The results with artificial linkers argue that, except for a minimal length requirement, the identity of the residues in the linker is rather unimportant in defining the inactivation competency of the NH_2 terminus. However, one interesting aspect of the results was that both τ_{on} and τ_{off} were altered by changes in linker length. For the poly-Q linkers, the shorter linkers exhibited a more rapid onset of inactivation, representing a 2–3-fold change in $\tau_{on.}$ In contrast, for a change in poly-Q linker length from 13 to 30 residues, τ_{off} slowed ~10-fold. Similarly, the poly-P linkers produced a marked slowing in τ_{off} with increases in length. How might the linker influence both τ_{on} and τ_{off}?

On the whole, the changes in τ_{on} with linker length were rather minor compared with the changes in τ_{off}. Some changes in τ_{on} with linker length might be expected, if the degrees of freedom of movement of the NH_2 terminus depend on linker length. As the linker length is increased, the inactivation epitope may be less likely to approach its site of action. This suggests that the FIW segment can readily access its blocking position irrespective of the length of the linker. The importance of flexibility in the linker is also indicated by the difference in τ_{on} between poly-Q and poly-P linkers.

Perhaps more surprising is that linker length has such pronounced effects on $\tau_{off.}$ If interaction of the inactivation domain with its site of action is defined largely by the nature of the FIW residues, the properties of the linker would not be expected to have much effect on τ_{off}. In fact, for most of the NH_2-terminal mutations studied in this paper, including charge mutations, deletions, and insertions, τ_{off} is remarkably unaffected. The main exception to this is that mutations of residues in the FIW epitope can strongly increase recovery rate. For example, for all the ΔFI charge mutations, τ_{off} is within a factor of 2–3, while for mutations in the FIW epitope τ_{off} can vary as much as 20-fold from wild-type. In the case of mutations in the FIW epitope, the changes in τ_{off} are likely to arise from changes in affinity of the FIW segment for binding sites. However, all the poly-Q linkers share the same FIW segment. Why then does the length of the poly-Q linkers result in an up to 10-fold change in τ_{off}? One explanation might be that either steric constraints imposed by the shorter linkers or flexibility arising from the linker may impact on the dissociation of the inactivation epitope from its

binding site. An alternative explanation might be that, if blockade is occurring within the pore, the average position of occupancy by the inactivation epitope (FIW) within the pore may depend on the chain length or flexibility of the chain.

Another implication of the ability of the artificial NH_2 termini to support inactivation is that these results show that charge per se is absolutely not critical to the ability of an NH_2 terminus to produce inactivation. Thus, for inactivation mechanisms that involve two kinetic steps (Lingle et al., 2001; Zhou et al., 2001), it is highly unlikely that one step corresponds to the interaction of charged residues on the NH_2 terminus with residues lining the entrance to the pore as proposed for Kv channel (Zhou et al., 2001). In fact, consistent with this idea, we have been able to demonstrate that an inactivation epitope linked to TM1 with a poly-Q chain still exhibits two-step inactivation (unpublished data).

Summary

Although these results suggest that BK inactivation and Kv inactivation may share a generally similar mechanistic, several key issues remain to be resolved. First and foremost, if the β2 NH_2-terminal inactivation segment does cause inactivation by linear insertion into the permeation pathway, the position at which the FIW segment blocks and its relationship to deactivation in BK channels must be resolved. Second, linear entry of a peptide segment does not provide a simple explanation for the two kinetic steps observed in the inactivation mechanism. One possibility is that, as the linear peptide segment transits to its deepest blocking position, the peptide can transiently interact at different positions along the inner helix in some cases in positions that do not hinder ion permeation. Testing the general outline for BK inactivation presented here will clearly require elucidation of the topology of the cytosolic side of the BK channel, information that currently remains unavailable.

We thank Nui Dong for assistance in preparation of some of the constructs used in this work and we thank Lynn Lavack for technical assistance.

We thank the Department of Anesthesiology for support for most of this work and DK46564 for a portion of this work.

Olaf Andersen served as editor.

Submitted: 7 October 2002
Revised: 4 December 2002
Accepted: 7 January 2003

REFERENCES

Antz, C., M. Geyer, B. Fakler, M.K. Schott, H.R. Guy, R. Frank, J.P. Ruppersberg, and H.R. Kalbitzer. 1997. NMR structure of inactivation gates from mammalian voltage-dependent potassium channels. *Nature.* 385:272–275.

Bentrop, D., M. Beyermann, R. Wissmann, and B. Fakler. 2001. NMR structure of the ball-and-chain domain of KCNMB2, the β2-subunit of large conductance Ca^{2+}- and voltage-activated potassium channels. *J. Biol. Chem.* 45:42116-42121.

Choi, K.L., R.W. Aldrich, and G. Yellen. 1991. Tetraethylammonium blockade distinguishes two inactivation mechanisms in voltage-activated K^+ channels. *Proc. Natl. Acad. Sci. USA.* 88:5092–5095.

Creighton, T. 1993. Proteins. Structures and Molecular Properties. W.H. Freeman and Company, New York, NY.

del Camino, D., and G. Yellen. 2001. Tight steric closure at the intracellular activation gate of a voltage-gated K(+) channel. *Neuron.* 32:649–656.

Demo, S.D., and G. Yellen. 1991. The inactivation gate of the Shaker K^+ channel behaves like an open- channel blocker. *Neuron.* 7:743–753.

Ding, J., and C. Lingle. 2002. Steady-state and closed-state inactivation properties of inactivating BK channels. *Biophys. J.* 82:2448–2465.

Ding, J.P., Z.W. Li, and C.J. Lingle. 1998. Inactivating BK channels in rat chromaffin cells may arise from heteromultimeric assembly of distinct inactivation-competent and noninactivating subunits. *Biophys. J.* 74:268–289.

Foster, C.D., S. Chung, W.N. Zagotta, R.W. Aldrich, and I.B. Levitan. 1992. A peptide derived from the Shaker B K^+ channel produces short and long blocks of reconstituted Ca^{2+}-dependent K^+ channels. *Neuron.* 9:229–236.

Gomez-Lagunas, F., and C.M. Armstrong. 1994. The relation between ion permeation and recovery from inactivation of ShakerB K^+ channels. *Biophys. J.* 67:1806–1815.

Gomez-Lagunas, F., and C.M. Armstrong. 1995. Inactivation in ShakerB K^+ channels: a test for the number of inactivating particles on each channel. *Biophys. J.* 68:89–95.

Hamill, O.P., A. Marty, E. Neher, B. Sakmann, and F.J. Sigworth. 1981. Improved patch-clamp techniques for high-resolution current recording from cells and cell-free membrane patches. *Pflugers Arch.* 391:85–100.

Hollerer-Beitz, G., R. Schonherr, M. Koenen, and S.H. Heinemann. 1999. N-terminal deletions of rKv1.4 channels affect the voltage dependence of channel availability. *Pflugers Arch.* 438:141–146.

Hoshi, T., W.N. Zagotta, and R.W. Aldrich. 1990. Biophysical and molecular mechanisms of Shaker potassium channel inactivation. *Science.* 250:533–538.

Jiang, Y., A. Lee, J. Chen, M. Cadene, B.T. Chait, and R. MacKinnon. 2002. The open pore conformation of potassium channels. *Nature.* 417:523–526.

Knaus, H.G., K. Folander, M. Garcia-Calvo, M.L. Garcia, G.J. Kaczorowski, M. Smith, and R. Swanson. 1994a. Primary sequence and immunological characterization of beta-subunit of high conductance Ca^{2+}-activated K^+ channel from smooth muscle. *J. Biol. Chem.* 269:17274–17278.

Knaus, H.G., M. Garcia-Calvo, G.J. Kaczorowski, and M.L. Garcia. 1994b. Subunit composition of the high conductance calcium-activated potassium channel from smooth muscle, a representative of the mSlo and slowpoke family of potassium channels. *J. Biol. Chem.* 269:3921–3924.

Kondoh, S., K. Ishii, Y. Nakamura, and N. Taira. 1997. A mammalian transient type K^+ channel, rat Kv1.4, has two potential domains that could produce rapid inactivation. *J. Biol. Chem.* 272: 19333–19338.

Kramer, R.H., E. Goulding, and S.A. Siegelbaum. 1994. Potassium channel inactivation peptide blocks cyclic nucleotide-gated channels by binding to the conserved pore domain. *Neuron.* 12:655–662.

Kuo, C.C., and S.Y. Liao. 2000. Facilitation of recovery from inactivation by external Na^+ and location of the activation gate in neuronal Na^+ channels. *J. Neurosci.* 20:5639–5646.

Lingle, C., X.-H. Zeng, J.-P. Ding, and X.-M. Xia. 2001. Inactivation of BK channels mediated by the N-terminus of the β3b auxiliary subunit involves a two-step mechanism: possible separation of binding and blockade. *J. Gen. Physiol.* 117:583–605.

Lingle, C.J., C.R. Solaro, M. Prakriya, and J.P. Ding. 1996. Calcium-activated potassium channels in adrenal chromaffin cells. *Ion Channels.* 4:261–301.

MacKinnon, R., R.W. Aldrich, and A.W. Lee. 1993. Functional stoichiometry of Shaker potassium channel inactivation. *Science.* 262: 757–759.

Murrell-Lagnado, R.D., and R.W. Aldrich. 1993a. Energetics of Shaker K channels block by inactivation peptides. *J. Gen. Physiol.* 102:977–1003.

Murrell-Lagnado, R.D., and R.W. Aldrich. 1993b. Interactions of amino terminal domains of Shaker K channels with a pore blocking site studied with synthetic peptides. *J. Gen. Physiol.* 102:949–975.

O'Leary, M.E., and R. Horn. 1994. Internal block of human heart sodium channels by symmetrical tetra-alkylammoniums. *J. Gen. Physiol.* 104:507–522.

O'Neil, K.T., and W.F. DeGrado. 1990. A thermodynamic scale for the helix-forming tendencies of the commonly occurring amino acids. *Science.* 250:646–651.

Rasmusson, R.L., S. Wang, R.C. Castellino, M.J. Morales, and H.C. Strauss. 1997. The beta subunit, Kv beta 1.2, acts as a rapid open channel blocker of NH2-terminal deleted Kv1.4 alpha-subunits. *Adv. Exp. Med. Biol.* 430:29–37.

Rettig, J., S.H. Heinemann, F. Wunder, C. Lorra, D.N. Parcej, J.O. Dolly, and O. Pongs. 1994. Inactivation properties of voltage-gated K^+ channels altered by presence of beta-subunit. *Nature.* 369:289–294.

Rose, G., A. Geselowitz, G. Lesser, R. Lee, and M. Zehfus. 1985. Hydrophobicity of amino acid residues in globular proteins. *Science.* 229:834–838.

Ruppersberg, J.P., R. Frank, O. Pongs, and M. Stocker. 1991. Cloned neuronal IK(A) channels reopen during recovery from inactivation. *Nature.* 353:657–660.

Schott, M.K., C. Antz, R. Frank, J.P. Ruppersberg, and H.R. Kalbitzer. 1998. Structure of the inactivating gate from the Shaker voltage gated K^+ channel analyzed by NMR spectroscopy. *Eur. Biophys. J.* 27:99–104.

Solaro, C.R., J.P. Ding, Z.W. Li, and C.J. Lingle. 1997. The cytosolic inactivation domains of BK_i channels in rat chromaffin cells do not behave like simple, open-channel blockers. *Biophys. J.* 73: 819–830.

Solaro, C.R., and C.J. Lingle. 1992. Trypsin-sensitive, rapid inactivation of a calcium-activated potassium channel. *Science.* 257:1694–1698.

Solaro, C.R., M. Prakriya, J.P. Ding, and C.J. Lingle. 1995. Inactivating and noninactivating Ca^{2+}- and voltage-dependent K^+ current in rat adrenal chromaffin cells. *J. Neurosci.* 15:6110–6123.

Toro, L., E. Stefani, and R. Latorre. 1992. Internal blockade of a Ca^{2+}-activated K^+ channel by Shaker B inactivating "ball" peptide. *Neuron.* 9:237–245.

Tseng-Crank, J., J.A. Yao, M.F. Berman, and G.N. Tseng. 1993. Functional role of the NH2-terminal cytoplasmic domain of a mammalian A- type K channel. *J. Gen. Physiol.* 102:1057–1083.

Uebele, V.N., A. Lagrutta, T. Wade, D.J. Figueroa, Y. Liu, E. McKenna, C.P. Austin, P.B. Bennett, and R. Swanson. 2000. Cloning and functional expression of two families of beta-subunits of the large conductance calcium-activated K^+ channel. *J. Biol. Chem.* 275:23211–23218.

Wallner, M., P. Meera, and L. Toro. 1999. Molecular basis of fast inactivation in voltage and Ca^{2+}-activated K^+ channels: a transmembrane beta-subunit homolog. *Proc. Natl. Acad. Sci. USA.* 96: 4137–4142.

Wang, Y.-W., J.P. Ding, X.-M. Xia, and C.J. Lingle. 2002. Consequences of the stoichiometry of *Slo1* α and auxiliary β subunits on functional properties of BK-type Ca^{2+}-activated K^+ channels. *J. Neurosci.* 22:1550–1561.

Wissmann, R., T. Baukrowitz, H. Kalbacher, H.R. Kalbitzer, J.P. Ruppersberg, O. Pongs, C. Antz, and B. Fakler. 1999. NMR structure and functional characteristics of the hydrophilic N terminus of the potassium channel beta-subunit Kvbeta1.1. *J. Biol. Chem.* 274: 35521–35525.

Xia, X., B. Hirschberg, S. Smolik, M. Forte, and J.P. Adelman. 1998a. dSLo interacting protein 1, a novel protein that interacts with large-conductance calcium-activated potassium channels. *J. Neurosci.* 18:2360–2369.

Xia, X.M., J.P. Ding, and C.J. Lingle. 1999. Molecular basis for the inactivation of Ca^{2+}- and voltage-dependent BK channels in adrenal chromaffin cells and rat insulinoma tumor cells. *J. Neurosci.* 19:5255–5264.

Xia, X.M., B. Fakler, A. Rivard, G. Wayman, T. Johnson-Pais, J.E. Keen, T. Ishii, B. Hirschberg, C.T. Bond, S. Lutsenko, et al. 1998b. Mechanism of calcium gating in small-conductance calcium-activated potassium channels. *Nature.* 395:503–507.

Xia, X.-M., J. Ding, X.-H. Zeng, K.-L. Duan, and C. Lingle. 2000. Rectification and rapid activation at low Ca^{2+} of Ca^{2+}-activated, voltage-dependent BK currents: consequences of rapid inactivation by a novel β subunit. *J. Neurosci.* 20:4890–4903.

Zagotta, W.N., T. Hoshi, and R.W. Aldrich. 1990. Restoration of inactivation in mutants of Shaker potassium channels by a peptide derived from ShB. *Science.* 250:568–571.

Zeng, X.-H., X.-M. Xia, and C.J. Lingle. 2001. Gating properties conferred on BK channels by the β3b auxiliary subunit in the absence of its N- and C-termini. *J. Gen. Physiol.* 117:607–627.

Zhang, X., C. Solaro, and C. Lingle. 2001. Allosteric regulation of BK channel gating by Ca^{2+} and Mg^{2+} through a non-selective, low affinity divalent cation site. *J. Gen. Physiol.* 118:607–635.

Zhou, M., J.H. Morais-Cabral, S. Mann, and R. MacKinnon. 2001. Potassium channel receptor site for the inactivation gate and quaternary amine inhibitors. *Nature.* 411:657–661.